



Published in final edited form as:

Cell Rep. 2021 October 05; 37(1): 109769. doi:10.1016/j.celrep.2021.109769.

## CHD1 controls H3.3 incorporation in adult brain chromatin to maintain metabolic homeostasis and normal lifespan

Ines Schoberleitner<sup>1</sup>, Ingo Bauer<sup>1</sup>, Anming Huang<sup>1</sup>, Evgeniya N. Andreyeva<sup>2</sup>, Johanna Sebald<sup>1</sup>, Katharina Pascher<sup>1</sup>, Dietmar Rieder<sup>3</sup>, Melanie Brunner<sup>1</sup>, Valerie Podhraski<sup>1</sup>, Gregor Oemer<sup>4</sup>, Daniel Cázarez-García<sup>5</sup>, Leila Rieder<sup>1</sup>, Markus A. Keller<sup>4</sup>, Robert Winkler<sup>5</sup>, Dmitry V. Fyodorov<sup>2,\*</sup>, Alexandra Lusser<sup>1,6,\*</sup>

<sup>1</sup>Institute of Molecular Biology, Biocenter, Medical University of Innsbruck, Innsbruck 6020, Austria

<sup>2</sup>Department of Cell Biology, Albert Einstein College of Medicine, Bronx, NY 10461, USA

<sup>3</sup>Institute of Bioinformatics, Biocenter, Medical University of Innsbruck, Innsbruck 6020, Austria

<sup>4</sup>Institute of Human Genetics, Medical University of Innsbruck, Innsbruck 6020, Austria

<sup>5</sup>Department of Biotechnology and Biochemistry, Cinvestav Unidad Irapuato, Irapuato 36824, Mexico

<sup>6</sup>Lead contact

### SUMMARY

The ATP-dependent chromatin remodeling factor CHD1 is essential for the assembly of variant histone H3.3 into paternal chromatin during sperm chromatin remodeling in fertilized eggs. It remains unclear, however, if CHD1 has a similar role in normal diploid cells. Using a specifically tailored quantitative mass spectrometry approach, we show that *Chd1* disruption results in reduced H3.3 levels in heads of *Chd1* mutant flies. *Chd1* deletion perturbs brain chromatin structure in a similar way as *H3.3* deletion and leads to global de-repression of transcription. The physiological consequences are reduced food intake, metabolic alterations, and shortened lifespan. Notably, brain-specific CHD1 expression rescues these phenotypes. We further demonstrate a strong genetic interaction between *Chd1* and H3.3 chaperone *Hira*. Thus, our findings establish CHD1 as a factor required for the assembly of H3.3-containing chromatin in adult cells and suggest a crucial role for CHD1 in the brain as a regulator of organismal health and longevity.

This is an open access article under the CC BY-NC-ND license (<http://creativecommons.org/licenses/by-nc-nd/4.0/>).

\*Correspondence: dmitry.fyodorov@einsteinmed.org (D.V.F.), alexandra.lusser@i-med.ac.at (A.L.).

#### AUTHOR CONTRIBUTIONS

I.S., J.S., and A.L. conceived the project and designed the experiments. I.S., A.H., J.S., K.P., and V.P. performed phenotype characterization experiments. I.B., D.R., and L.R. analyzed NGS data. G.O., D.C.G., M.A.K., and R.W. performed metabolite mass spec experiments and data analysis. M.B. isolated histones. E.N.A. and D.V.F. developed H3.3 quantification by MRM-HR. A.L. performed ATAC-seq experiments. A.L., D.V.F., and I.S. analyzed the data and wrote the manuscript with help from I.B., M.A.K., R.K., and E.N.A.

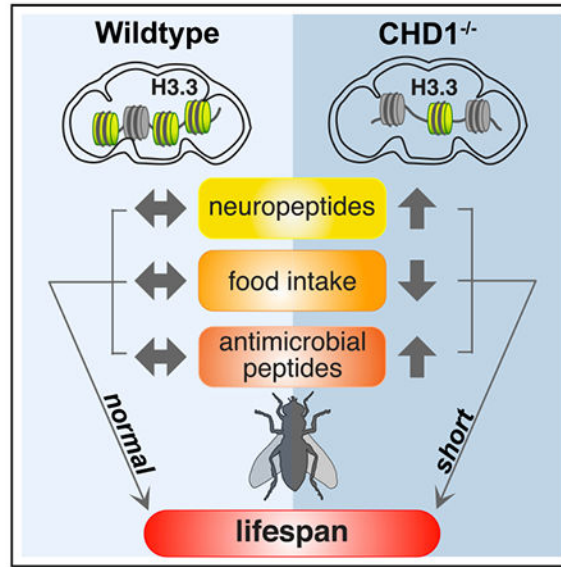
#### SUPPLEMENTAL INFORMATION

Supplemental information can be found online at <https://doi.org/10.1016/j.celrep.2021.109769>.

#### DECLARATION OF INTERESTS

The authors declare no competing interests.

## Graphical abstract



## In brief

In postmitotic brain cells, histones lost during transcription must be replenished by replication-independent mechanisms. Schoberleitner et al. show that the chromatin remodeling factor CHD1 is involved in this process. CHD1 loss results in reduced histone H3.3 levels, global chromatin perturbation, transcriptional dysregulation, and defects in feeding behavior, metabolism, and lifespan.

## INTRODUCTION

The chromodomain-helicase-DNA binding protein 1 (CHD1) belongs to the Snf2 superfamily of ATP-utilizing motor proteins whose primary function is to modulate histone-DNA contacts within and between nucleosomes in chromatin (Clapier and Cairns, 2009). Chromatin remodeling factors are critical components of all processes that require access to the DNA substrate, most prominently transcription, replication, and DNA damage repair, and they are major effectors of chromatin dynamics. CHD1 was shown to move nucleosomes and hexasomes (lacking one H2A/H2B dimer) in a directional manner (Levendosky et al., 2016; Qiu et al., 2017; Rippe et al., 2007; Stockdale et al., 2006). Additionally, CHD1 can facilitate *in vitro* the assembly of nucleosomes into regularly spaced arrays (Lusser et al., 2005). The ATP-dependent assembly activity of CHD1 can be biochemically separated from its remodeling activity because a remodeling-defective mutant can still promote nucleosome formation (Torigoe et al., 2013). It has been proposed that the assembly of nucleosomes is mediated in concert by core histone chaperones and ATP-dependent motor factors such as CHD1 (Lusser and Kadonaga, 2004). A recent model suggests that whereas the histone chaperones are essential for histone delivery to the sites of chromatin assembly and the initial deposition of an immature “pre-nucleosome” particle, the

ATP-dependent motor completes its folding into a canonical nucleosome (Fei et al., 2015; Torigoe et al., 2011).

The biological roles of CHD1 have been studied in various organisms. CHD1 is involved in transcription-independent as well as at multiple stages of transcription-related processes. The majority of studies has focused on its role in transcription regulation demonstrating that it is primarily associated with transcriptionally active locations throughout the genome (de Dieuleveult et al., 2016; Gaspar-Maia et al., 2009; Lin et al., 2011; Morettini et al., 2011; Siggins et al., 2015; Simic et al., 2003; Srinivasan et al., 2008). CHD1 promotes RNAP II promoter escape (Petesch and Lis, 2008; Skene et al., 2009), and deletion of yeast *chd1* decreased nucleosome positioning and/or occupancy over coding regions and promoted the use of cryptic promoters (Hennig et al., 2012; Lee et al., 2012; Quan and Hartzog, 2010; Smolle et al., 2012). In mouse embryonic stem cells, *Chd1* deletion resulted in general downregulation of transcription by RNAP II and I (Guzman-Ayala et al., 2015). CHD1 was further found to affect splicing (Lee et al., 2017; Sims et al., 2007) and transcription termination (Alén et al., 2002; Radman-Livaja et al., 2012).

CHD1 is essential for global transcription- and replication-independent histone H3.3 incorporation into paternal pronuclear chromatin in *Drosophila* and the bovine system (Konev et al., 2007; Zhang et al., 2016). Unlike canonical histone H3.1/H3.2 that are expressed exclusively during S phase and are substrates for replication-dependent chromatin assembly, the H3.3 variant is considered a “replacement”-type histone, because it is deposited in a replication-independent manner, for instance during nucleosome re-assembly in the wake of transcribing polymerases (Talbert and Henikoff, 2010). Chromatin loading of H3.3 was shown to involve the two distinct histone chaperone complexes ATRX/DAXX and HIRA. The chaperone DAXX and the chromatin remodeling factor ATRX (XNP in *Drosophila*) cooperate to assemble H3.3 at telomeres and pericentric heterochromatin (Drané et al., 2010; Goldberg et al., 2010). The mammalian HIRA complex consists of HIRA, ubinuclein (UBN; yemanuclein in flies) and calcineurin-binding protein-1 (CABIN1; no homolog in flies) and mostly regulates the incorporation of H3.3 at active regions (Pchelintsev et al., 2013). Mammalian replication protein A (RPA) also cooperates with HIRA for H3.3 deposition (Zhang et al., 2017). In *Drosophila*, the HIRA complex, similar to CHD1, is essential for replication-independent loading of H3.3 into paternal chromatin (Bonney et al., 2007; Loppin et al., 2005; Orsi et al., 2013).

Nevertheless, although the loss of CHD1 in mammalian cells reduces nucleosome occupancy in the body of transcribed genes (Skene et al., 2009) and at transcriptional start sites (Siggins et al., 2015), a function for CHD1 in H3.3 incorporation in somatic cells beyond the specialized physiological situation in the early embryo has not been demonstrated.

In this work, we address this question by analyzing the effects of *Chd1* deletion on H3.3 incorporation in the brain of *Drosophila melanogaster*. Adult fly brains are composed mostly of postmitotic diploid cells and must rely exclusively on histone-variant-specific assembly mechanisms for histone turn-over. Thus, brain cells should be particularly sensitive to

potential H3.3 deposition defects caused by the absence of CHD1, whereas in other cell types, such effects might be obscured by incorporation of canonical H3.1 during replication.

## RESULTS

### Development of a liquid chromatography-tandem mass spectrometry (LC-MS/MS)-based method to quantify H3.3 levels in adult fly heads

To examine H3.3 loading into brain chromatin, we sought to measure its amounts in chromatin from heads of *Chd1* mutant and wild-type flies. Because of the limiting input material, we established a method allowing for sensitive quantification of the relative amounts of H3.3 and H3.1. To this end, we employed scheduled high-resolution multiple reaction monitoring (MRM-HR) (Schilling et al., 2015) mass spectrometry focusing on peptides derived from the region between amino acid positions 87–90, which specifies H3 variants (Figure 1A). To build the spectral library for MRM-HR, we performed extensive sequence analyses of *Drosophila* H3 protein by information-dependent acquisitions (IDA) with highly purified chromatin-derived histones from embryo that were separated by SDS-PAGE (Figure S1). We discovered that digestion with pepsin produces complete cleavage of the peptide bonds C-terminally of L82 and L92 in H3.1 and H3.3. No peptides spanning L82–R83 or L92–Q93 were detected. In addition to the decapeptides (R83–L92), we observed several peptides of 7–9 amino acids (Table S1) that, presumably, represent mis-cleavage products. However, we found no other shorter peptides starting at R83 (within the mass detection limit,  $m/z$  300). Finally, there was no evidence in the IDA spectra for peptides that could have been produced by cleavage at F84. Thus, 7–10 amino acid-long peptides with a charge state ( $z$ ) of 2 starting at R83 represent the complete repertoire of pepsin cleavage products of H3.1 and H3.3 in this diagnostic region, and their relative quantification must reflect the physiological ratio of the proteins.

Refinement of the MRM-HR method by acquisitions on various amounts of purified embryonic H3 (Figure 1B) revealed a robust pattern of specific ions (Table S1) that allowed for automated peak calling by Skyline and subsequent calculation of H3.3/H3.1 ratios. We determined that H3.3 represents  $12.2\% \pm 0.1\%$  of total H3 purified from *Drosophila* embryos. This result was highly reproducible even with input amounts as low as 20 ng (Figure 1C). To examine the compatibility of this procedure with less pure preparations of H3, we isolated histones from whole adult flies or fly heads (Figure S1). The utilized procedure also eliminated extra- and pre-nucleosomal components of the nuclei (see STAR Methods) enabling measurement of nucleosomal H3. Gel slices (>20 ng total H3 at ~25% purity) were subjected to MRM-HR analyses. We obtained highly reproducible results for relative H3.3 content with little variation across biological replicates. Interestingly, although the overall levels of H3.3 in whole adult female flies were similar to those of embryos, adult males exhibited a slight but significant increase in H3.3 ( $14.2\% \pm 0.3\%$  versus  $12.2\% \pm 0.7\%$ ; Figure 1C). The latter is likely owed to a high number of actively (endo)replicating cells in the female ovaries. Consistently, chromatin of fly heads with their high prevalence of postmitotic brain cells exhibited a steady age-dependent increase of H3.3 reaching ~40% of total H3 by 40 days of age (Figure 1D).

### Absence of CHD1 leads to severely decreased histone H3.3 levels in brain chromatin

We then prepared chromatin extracts from the heads of 20-day-old females bearing deletions in both *Chd1* alleles (*Chd1<sup>1</sup>/Df(2L)Exel<sup>7041</sup>*; hereafter termed *Chd1<sup>-/-</sup>*) and of *Chd1<sup>-/-</sup>* flies expressing *Chd1* from a transgene under the control of its native promoter (*Chd1<sup>1</sup>, P{F-Chd1}/Df(2L)Exel<sup>7041</sup>, P{F-Chd1}*); hereafter termed *Chd1<sup>WT/WT</sup>*) (Table 1). We extracted chromatin-bound histones and measured SDS-PAGE-separated H3 containing bands (Figure S1) by MRM-HR. The results show that the absence of CHD1 caused an almost 2-fold reduction of relative H3.3 levels ( $12.7\% \pm 0.9\%$ ) compared to *Chd1<sup>WT/WT</sup>* heads ( $22.3\% \pm 1.3\%$ ) (Figure 1E). When we reintroduced *Chd1* expression in the brain of *Chd1<sup>-/-</sup>* flies by the pan-neuronal *elav-Gal4* driver (*Chd1<sup>elav</sup>*) (Table 1; Figure S2A), H3.3 was restored to wild-type levels (Figure 1E). These findings indicate that CHD1 is required for H3.3 incorporation into chromatin of adult fly heads.

### Contribution of H3.3 chaperone HIRA

Even though our data reveal a striking decrease of H3.3 in brain chromatin of *Chd1* mutants, H3.3 is not completely absent. This is likely owed to cooperation of CHD1 with dedicated histone chaperones, such as HIRA, as is the case in pronuclear chromatin remodeling (Konev et al., 2007; Loppin et al., 2005). Thus, the chaperone likely deposits H3.3 to some extent whereas CHD1 might be necessary to improve the efficiency of the assembly and to organize proper nucleosome spacing (Figure 2A) (Fei et al., 2015; Lusser et al., 2005; Torigoe et al., 2011). To examine this idea, we crossed *Chd1<sup>-/-</sup>* flies with *ssm<sup>185b</sup>* flies that bear a loss of function mutation in the *Hira* gene (Loppin et al., 2005; 2000). The results show that combined homozygous null mutation of *Chd1* and *Hira* is synthetic lethal, whereas viability is largely unaffected as long as one intact allele of either gene remains (Figure 2B), thus supporting the mode of action proposed above.

Because CHD1 is a known transcriptional regulator, however, its absence might also interfere with the expression of *Hira* or other factors that can mediate H3.3 deposition or of H3.3 itself. Thus, we analyzed global gene expression in heads of *Chd1<sup>-/-</sup>*, *Chd1<sup>WT/WT</sup>*, and *Chd1<sup>elav</sup>* flies by RNA sequencing (RNA-seq). PCA analysis revealed segregation of the different genotypes and high correlation between biological replicates (Figure S3A). The expression levels of the H3.3 encoding genes *His3.3A* and *His3.3B* or of the known H3.3 assembly factors, including *Hira*, varied between a log<sub>2</sub> fold change (l2fc) of 0.16 for *His3.3B* and 0.88 for *Hira* and, thus, were below the typical l2fc threshold of 1 (−1) for differentially regulated genes (Figure S2B). Likewise, western blot analysis of head protein extracts with antibodies detecting the H3.3 chaperones HIRA and ASF1 and the chromatin remodeler XNP revealed similar amounts in *Chd1<sup>-/-</sup>* and *Chd1<sup>WT/WT</sup>* flies (Figures 2C and 2D). Combined, our results therefore support a direct role for CHD1 in H3.3 incorporation into chromatin of adult fly brain, a tissue that is expected to be particularly sensitive to defects in replication-independent nucleosome assembly mechanisms.

### Absence of CHD1 causes widespread transcriptional dysregulation in the brain

CHD1 is generally considered a transcriptional activator (Guzman-Ayala et al., 2015; Morettini et al., 2011; Skene et al., 2009), and gene expression analyses in other organisms as well as our own previous analysis of *Chd1* mutant larvae revealed fairly similar numbers

of up- and downregulated genes (e.g., Augello et al., 2019; Sebald et al., 2012). Surprisingly, when we examined the RNA-seq data from *Drosophila* heads in more detail, we discovered that in *Chd1* mutants, the number of expressed genes was ~15% higher than in *Chd1<sup>WT/WT</sup>* or *Chd1<sup>elav</sup>* flies (Figure 3A). Furthermore, we found that of the ~4,000 genes that showed significant differential expression (12fc 1, p.adj 0.05), the vast majority was in fact upregulated in *Chd1* mutant heads compared to either *Chd1<sup>WT/WT</sup>* or *Chd1<sup>elav</sup>* samples (Figure 3B; Tables S2 and S3). In light of these findings, we hypothesized that the reduction of chromatin-bound H3.3 in *Chd1* mutant flies may lead to a general relaxation of chromatin-imposed transcriptional repression.

To investigate this hypothesis, we analyzed the state of the chromatin by ATAC-seq (assay for transposase-accessible chromatin using sequencing; Buenrostro et al., 2013; Davie et al., 2018) on isolated brains from 10-day-old female *Chd1<sup>WT/WT</sup>* and *Chd1<sup>-/-</sup>* flies (Figure S3B). In addition, we used a fly strain that lacks both histone H3.3 genes (*H3.3 KO*) (Hödl and Basler, 2009) because we reasoned that chromatin alterations in these flies should resemble those of *Chd1<sup>-/-</sup>* flies. We found substantial changes in chromatin accessibility, with loss and gain of several hundred peaks in the absence of either CHD1 or H3.3 (Figure 3C). New peaks in *Chd1<sup>-/-</sup>* flies had a very slight preference for upregulated genes compared to non-regulated genes, while the reverse was true for lost peaks (Table S4). Interestingly, despite higher numbers of mapped reads, the total number of peaks in both *Chd1<sup>-/-</sup>* and *H3.3 KO* brains was reduced compared to wild-type (Figures S3C and S3D), and the relative distribution of ATAC-peaks was changed. In wild-type brains the majority of peaks was found in promoters/transcriptional start sites and introns and only 10% in exonic regions, the latter fraction increased in *Chd1* mutant flies to ~18% and to ~24% in *H3.3 KO* mutants (Figure S3E). Peak intensities were reduced in the absence of CHD1 as well as in *H3.3 KO* mutants (Figures 3D and S3F). These observations seem counterintuitive because if the defective H3.3 loading caused a more open chromatin structure, a greater number of peaks would be expected. It is possible, however, that a general opening of the chromatin structure leads to more broadly distributed tagmentation events during the ATAC procedure resulting in reduced peak calling. To investigate this possibility, we examined ATAC-read distribution around transcriptional start sites. Four clusters with distinct read distribution patterns were identified, and in all clusters, *Chd1<sup>-/-</sup>* and *H3.3 KO* brains exhibited a remarkable increase of read densities across gene bodies (Figure 3E) suggesting enhanced chromatin accessibility.

Together, the data show that chromatin changes occurring in *Chd1<sup>-/-</sup>* brains resemble those of *H3.3 KO* mutants providing further support for the involvement of CHD1 in H3.3 incorporation particularly in genic regions. Of note, the assay for transposase-accessible chromatin using sequencing (ATAC-seq) data also revealed an interesting difference between *Chd1<sup>-/-</sup>* and *H3.3 KO* brains. The latter showed a pronounced accessibility increase of pericentromeric regions compared to *Chd1<sup>-/-</sup>* or *Chd1<sup>WT/WT</sup>* brains (Figure S3G) indicating that activities other than CHD1 mediate the assembly of H3.3 in those regions. This is consistent with previous reports of H3.3 incorporation in pericentromeric regions being achieved by ATRX/DAXX (Drané et al., 2010; Goldberg et al., 2010).

## CHD1 regulates the expression of metabolism control genes in the brain

To understand the functional implications of transcriptional dysregulation in *Chd1* mutant brain, we searched for enriched gene categories. G-protein-coupled signaling and neuropeptide signaling scored among the terms with the highest significance (Figure 3F). Closer inspection revealed that many neuropeptides and other proteins known to regulate hunger and satiety were among the genes upregulated in *Chd1* mutant flies when compared to both *Chd1<sup>WT/WT</sup>* and *Chd1<sup>elav</sup>* flies (Figure S4). For instance, the genes encoding *Allatostatin A Receptor 1 (AstA-RI)*, *AstC*, *Hugin (Hug)* or *Drosulfakinin (Dsk)* showed higher expression in *Drosophila* heads in the absence of CHD1 compared to when CHD1 was expressed under the control of its native promoter (*Chd1<sup>WT/WT</sup>*) or under the *elav* promoter (*Chd1<sup>elav</sup>*) (Figure S4). These factors have been linked to negative control of food intake (Lin et al., 2019). Along the same lines, *Drosophila insulin-like peptides (ILPs) 2, 3, and 5* were significantly upregulated in *Chd1<sup>-/-</sup>* compared to both *Chd1<sup>WT/WT</sup>* and *Chd1<sup>elav</sup>* flies (Figure S4). These ILPs are expressed in specific neurons in the fly brain and function, among other things, as satiety signals that negatively affect feeding motivation. On the other hand, we also detected increased transcript levels of genes encoding hunger signaling proteins and peptides, such as *AKH*, *SIFamide (SIFa)* or *SIFamide receptor (SIFaR)*, *neuropeptide F (NPF)*, or *small NPF (sNPF)* (Lin et al., 2019).

Moreover, genes involved in immune response were among the most significantly enriched categories in Gene Ontology (GO) analysis (Figure S4). Many of these genes (e.g., the antimicrobial peptide [AMP] genes *Attacin A-D*, *Cecropin A1-C*, or *Diptericin B*) are predominantly expressed in peripheral tissues, such as the fat body or intestinal and tracheal epithelia. Because our RNA-seq analysis was performed with RNA from fly heads, it is possible that the detected transcripts might have originated from head fat body tissue and/or brain cells.

With respect to chromatin accessibility alterations in the absence of CHD1, we found that the GO term *neuropeptides* was significantly enriched only among dysregulated genes of ATAC-seq cluster 4 (Figure S5A). Likewise, many differentially regulated immune response-related genes were present in this cluster. IGV tracks of example neuropeptide genes, such as the *Ilp* cluster (containing upregulated *Ilp3* and *Ilp2*), *AstC*, *Akh*, or the AMP genes *Mtk*, *AttD*, or *CecB*, revealed that, typically, chromatin accessibility was increased over the gene body compared to wild-type brains. Of note, the increased accessibility was also observed in *H3.3 KO* mutant brains (Figure S5B). These results point toward a role of CHD1 in controlling chromatin structure in transcribing loci likely by facilitating the reassembly of H3.3-containing nucleosomes in the event of nucleosomal loss during transcription. Importantly, they do not rule out additional functions of CHD1, such as remodeling of nucleosomes in promoter regions.

Taken together, the characteristics of the most prominently affected genes in *Chd1<sup>-/-</sup>* flies suggest that the flies may suffer from metabolic disruption and exhibit a state of chronic low-grade inflammation.

## CHD1 affects feeding behavior and lifespan in *Drosophila melanogaster*

Given the dysregulation of many hunger and satiety signaling neuropeptides, we examined the feeding behavior of *Chd1*<sup>-/-</sup> flies. To this end, we measured consumption of dyed food by flies of different ages (4, 14 days). We found that both young (4 days) as well as older (14 days) *Chd1* mutant flies consumed significantly less food than their wild-type counterparts (Figure 4A). Similarly, we observed severely decreased *ad libitum* food and water intake employing the capillary feeder (CAFE) assay (Deshpande et al., 2014), particularly in younger (4, 7 days) flies, although the difference was less pronounced in older flies (Figure 4B). These differences were reflected in reduced wet (-6.8%) and dry (-17.6%) body mass of *Chd1*<sup>-/-</sup> compared to *Chd1*<sup>WT/WT</sup> flies (Figure 4C). Thus, absence of CHD1 appears to disrupt normal feeding behavior likely due to dysregulation of feeding control mechanisms in the brain.

Because caloric restriction is considered one of the major factors extending lifespan in various organisms (Fontana and Partridge, 2015), we next examined potential effects of reduced food intake on the lifespan of *Chd1*<sup>-/-</sup> flies. Unexpectedly, we observed a severe decrease of median lifespan of *Chd1*<sup>-/-</sup> flies to 37 ± 2.88 days compared to *Chd1*<sup>WT/WT</sup> flies (median survival of 76 ± 2.33 days) (Figure 4D). Lifespan shortening was also observed for homozygous and transheterozygous but not for heterozygous combinations of the *Chd1*<sup>1</sup> and *Chd1*<sup>3</sup> (Konev et al., 2007) alleles (Figures 4E and S6A). These results suggest that the extent of food intake reduction apparently exceeds the benefits of calorie restriction and instead appears to result in starvation and death. Notably, when we overexpressed the hunger signaling factor sNPF in the brain of *Chd1*<sup>-/-</sup> flies, lifespan was fully rescued (Figure S6B) and food intake increased moderately (Figure S6C).

## Loss of CHD1 leads to altered metabolic profile and gradual depletion of metabolite stores

To examine the overall physiological consequences of reduced food consumption of *Chd1* mutant flies, we performed metabolic profiling of *Chd1*<sup>-/-</sup> and *Chd1*<sup>WT/WT</sup> flies. We obtained 87 features for principal component analysis revealing clear separation of *Chd1* mutant and wild-type genotypes (Figure 5A). This was further confirmed by hierarchical clustering analysis (Figure S7), indicating distinct metabolic identities of the two strains. Although a number of identified features was tentatively assigned to different lipid classes (Table S5), several polar metabolites were not accessible to mass fragmentation but could be identified as amino acids. We detected substantial differences in the abundance of various amino acids (Figure 5B) indicating considerable impact of the absence of CHD1 on the metabolic state of *Drosophila*.

We then analyzed circulating and stored carbohydrates and lipids. *Drosophila* hemolymph contains two major types of circulating sugars: glucose obtained from the diet and trehalose that originates in the fat body (Reyes-DelaTorre et al., 2012). Both are involved in a variety of functions. Glucose serves as an essential energy source in glycolysis and as a substrate for biosynthetic processes during growth and for energy storage through conversion into glycogen. Trehalose is a critical provider of energy for brain function and the flight muscle but also protects against environmental stress (Reyes-Dela Torre et al., 2012). Unexpectedly, levels of circulating glucose and trehalose in the hemolymph of 4-, 14-,

and 30-day-old female flies were increased in the youngest (4 days) and oldest (30 days) *Chd1*<sup>-/-</sup> flies. Only in 14-day-old flies, levels were comparable to the wild-type (Figure 5C). For trehalose, levels were significantly higher also in 4-day-old *Chd1* mutant flies, whereas they dropped below wild-type levels at 14 days of age and were similar to wild-type in 30-day-old flies (Figure 5C). The storage metabolite glycogen, by contrast, gradually decreased with age in *Chd1* mutant compared to wild-type flies (Figure 5D). Concordantly, the major storage lipid triacylglycerol (TAG) was strongly decreased in mutant flies (Figure 5D). We also examined the composition of cardiolipins (CLs), which are integral components of the inner mitochondrial membrane and have crucial impact on the assembly and function of respiratory chain protein complexes, thus contributing to cellular energy supply. The structural diversity of CLs is dependent on nutritional conditions (Oemer et al., 2018). High-performance liquid chromatography tandem mass spectrometry (HPLC-MS/MS) analysis confirmed the unique sex-specific *Drosophila* cardiolipidome (Oemer et al., 2018), consisting almost exclusively of FA14:0, FA16:1, FA18:1, and FA18:2 acyl chains (Figure S8). In contrast to wild-type flies, however, *Chd1* mutants displayed a clear shift toward increased carbon chain length and extent of saturation (Figure 5E), which may affect the stability of CLs and thus the functionality of mitochondrial oxidative phosphorylation (Xu et al., 2019). Taken together, the results illustrate that *Chd1* mutant flies suffer from severe disruption of global metabolism, including carbohydrates, amino acids, lipids, and cardiolipins.

### TOR pathway inhibition partially rescues shortened lifespan in *Chd1* mutant flies

The results suggested disturbed nutrient homeostasis in the absence of CHD1. Even though mutant flies consumed significantly less than their wild-type counterparts, circulating sugars were elevated, which might result from enhanced mobilization of glycogen and lipid stores combined with a defect in cellular sugar uptake from the hemolymph. The key hormones regulating metabolic balance are insulin (ILPs) and glucagon (AKH in flies), and insulin signaling has many links to TOR signaling (Antikainen et al., 2017). Because we observed increased ILP transcript levels (Figure S4), we speculated that TOR signaling might be aberrantly activated in *Chd1*<sup>-/-</sup> flies. Because TOR inhibition promotes longevity in different organisms and also affects food intake behavior (Antikainen et al., 2017; Ribeiro and Dickson, 2010), we investigated potential effects of TOR inhibition by rapamycin. We found that keeping the flies on food supplemented with rapamycin extended the median lifespan of *Chd1* mutant flies from 37 to 50.7 days (Figure 5F; Table S6). However, maximum lifespan was still substantially shorter in *Chd1* mutant compared to wild-type flies on standard food (Table S6). We also found that TOR inhibition reverted food intake of 4-day-old *Chd1* mutant flies to wild-type levels under standard dietary conditions (Figure 5G). Yet this effect was not persistent in older animals, which might explain the only partial rescue of the lifespan of *Chd1*<sup>-/-</sup> flies. Nevertheless, rapamycin treatment restored glycogen and TAG stores in 4- and 14-day-old *Chd1* mutants. Only in 30-day-old flies was a trend toward glycogen depletion and significant TAG depletion observed for the mutants (Figure 5H). Hence, inhibition of TOR signaling is able to transiently promote food intake of *Chd1* mutant flies that may be the cause for partial rescue of their lifespan. Of note, the lack of rapamycin-induced longevity-promoting effects observed for *Chd1*<sup>WT/WT</sup> flies is likely due to the high concentrations (200  $\mu$ M) (Harrison et al., 2010) that had to be used for

*Chd1*<sup>-/-</sup> flies to take up sufficient levels. Concentrations typically used in the literature (10 μM) (Schinaman et al., 2019) promoted lifespan extension in *Chd1*<sup>WT/WT</sup> flies (Figures S9A–S9C). In sharp contrast to rapamycin, dietary intervention (i.e., keeping flies on low sugar/high protein or high sugar/low protein diet) had no beneficial effect on lifespan or consumption (Figures S9D–S9H). Taken together, the data suggest that in the absence of CHD1, aberrant TOR signaling may play a role in lifespan regulation, presumably by affecting eating behavior of the fly.

### Brain-specific expression of CHD1 is crucial for normal feeding and lifespan

Next, we sought to examine whether the observed defects in *Chd1*<sup>-/-</sup> flies were linked to its role in the brain described above or whether functions of CHD1 in the periphery were responsible. To distinguish between these possibilities, we analyzed consumption and lifespan in *Chd1*<sup>elav</sup> flies. Indeed, brain-specific expression of *Chd1* was sufficient to fully rescue the consumption deficit (Figure 6A). Notably, even abdominal expression of the metabolic transcription factor *Sugarbabe* (*Sug*), which was downregulated in the abdomen of *Chd1* mutant flies, was restored by brain-specific expression of CHD1 (Figure 6B). *Sug* controls sugar-dependent repression of starch break-down as well as the generation of lipid stores (Mattila et al., 2015), and its downregulation in *Chd1* mutant flies may underlie the observed depleted TAG and glycogen stores (Figures 5C and 5D). Strikingly, brain-specific expression of *Chd1* fully restored lifespan. Median lifespan of *Chd1*<sup>elav</sup> was equal to *Chd1*<sup>WT/WT</sup> flies and significantly higher than that of *Chd1*<sup>-/-</sup> flies (Figure 6C).

Because several reports have linked elevated transcription of antimicrobial peptide genes to aging and lifespan (Landis et al., 2004; Rera et al., 2012; Wang et al., 2020), and because we had previously observed increased AMP levels in the gut of *Chd1* mutant flies (Sebald et al., 2012), we also examined the expression levels of the three AMPs *Metchnikowin* (*Mtk*), *Attacin C* (*AttC*), and *Drosomycin 3* (*Dro3*) in the abdomen of *Chd1*<sup>elav</sup> and control flies. We found that the dysregulation of the AMPs in the fly abdomen was significantly attenuated (Figure 6D). Thus, the activity of CHD1 in the brain is sufficient to restore normal eating behavior and lifespan and to prevent a state of chronic inflammation (elevated AMP expression) in the gut.

## DISCUSSION

We have previously demonstrated that CHD1 directs global H3.3 incorporation in paternal pronuclear chromatin and suggested a mechanism in which the chaperone HIRA cooperates with CHD1 by delivering H3.3 to the sites of incorporation, while CHD1 ensures efficient deposition and spacing (Konev et al., 2007). Although the role of HIRA in H3.3 assembly has been confirmed in other cellular contexts, CHD1 has not been noted as a general H3.3 assembly factor (Bano et al., 2017; Grover et al., 2018; Martire and Banaszynski, 2020). This may be due to the fact that most somatic cells undergo at least some degree of proliferation, in the course of which nucleosomes are replenished in a replication-coupled manner. The brain, by contrast, should be highly sensitive to defects in the H3.3 incorporation machinery because terminally differentiated neurons cannot replace histones/nucleosomes lost during transcription by DNA replication-coupled mechanisms. Indeed,

our data reveal that the absence of CHD1 causes a significant reduction of H3.3 in brain chromatin, alterations in chromatin accessibility, in particular over genic regions, and global transcriptional de-repression, thus strongly supporting a role for CHD1 in H3.3 assembly. In fact, complete knockout of *H3.3*-encoding genes had similar effects on brain chromatin organization as *Chd1* deletion. Furthermore, the fact that H3.3 is reduced but not eliminated from *Chd1* mutant chromatin, as well as the synthetic lethal genetic interaction between *Chd1* and *Hira*, are consistent with a model of CHD1 and HIRA functioning cooperatively in H3.3 deposition (Figure 2A) in adult brain and likely in other tissues. Thus, in the absence of CHD1, HIRA may be able to deposit H3.3, yet with reduced efficiency and impaired nucleosome spacing. A similar mechanism was also observed *in vitro* for the chromatin assembly factors CHD1 and ACF and the histone chaperone NAP1 (Fei et al., 2015; Lusser et al., 2005; Torigoe et al., 2011).

As pointed out by a reviewer of this study, our data—although highly suggestive—do not directly prove that CHD1-mediated H3.3 deposition is the (sole) activity responsible for the obtained phenotypes. It is possible that the transcriptional defects are caused by other chromatin remodeling-related functions of CHD1. Thus, it is useful to keep in mind that the loss of *Chd1* might also result in aberrant organization of nucleosomes in genic regions, defective incorporation of other types of histone-variants, and/or misexpression of H3.3 assembly factors or other specific regulatory proteins, and those defects, rather than reduced H3.3 levels, could lead to the observed widespread transcriptional upregulation in the brain.

### The role of CHD1 in the regulation of metabolism and lifespan

Among the groups of genes that were particularly affected by *Chd1* deletion were genes involved in neuropeptide signaling (Figure 6E). Because organismal health is dependent on strategies to maintain energy homeostasis in the face of constantly changing energy needs and nutritional supply, animals rely on a complex system of neuronal signals to translate the need for nutrients into behavioral output (i.e., foraging and feeding) (Lin et al., 2019). Thus, imbalance of neuronal signaling in the absence of CHD1 likely is the reason for aberrant feeding behavior, several manifestations of metabolic disruption and severe lifespan shortening (Figure 6E). For instance, we detected elevated expression levels of *ILPs 2, 3*, and *5* as well as of the glucagon analog *AKH* that were restored upon neuron-specific re-introduction of CHD1. ILPs and AKH are the best studied neuropeptide groups in the fly, and their mutually antagonistic impact on metabolism and lifespan is well-documented (Broughton et al., 2005; Giannakou and Partridge, 2007; Nässel and Zandawala, 2019; Tatar et al., 2001). Aberrantly increased ILP levels may contribute to reduced food intake in *Chd1* mutant flies by direct effects on feeding behavior and/or by upregulating TOR pathway. In fact, the partial rescue of consumption and lifespan upon TOR pathway inhibition, but not upon dietary intervention (low/high sugar diet), suggest that the observed anorexic phenotype has behavioral rather than metabolic causes. It will be interesting to elucidate the exact role of TOR in this context in future studies.

### *Chd1* deletion leads to chronic low-grade inflammation

In addition to the effect of CHD1 on neuropeptide signaling, we also observed signs of chronic inflammation in the absence of CHD1 reflected in elevated levels of immunity-

associated transcripts in the head of *Chd1* mutants (Figure 6E). Interestingly, neuronal expression of CHD1 restored AMP transcription to normal levels, not only in the head but also in the fly gut. The latter may be explained by the fact that food intake is largely rescued in these flies. The relationship between feeding, intestinal immune response, intestinal microbiome, and aging has been studied extensively (Erkosar and Leulier, 2014; Galenza and Foley, 2019; Lee and Lee, 2014). The gut microbiome of the fly is predominantly shaped by the ingested food, and intestinal AMP production in turn is affected by the microbiota. *Chd1* mutant flies have a disturbed intestinal microbiome and elevated intestinal AMP levels (Sebald et al., 2012; 2016). Moreover, the flies' food-intake is compromised and lifespan is shortened. Together, these phenotypes fit the prevalent view that bacterial dysbiosis and increased inflammation (i.e., elevated AMP expression) in the gut are hallmarks of aging (Clark and Walker, 2018; Galenza and Foley, 2019). Chronic low-grade inflammation has also been linked to aging in humans (“inflammaging”) (Franceschi et al., 2018), and it likely also contributes to shortened lifespan in *Chd1* mutant flies (Figure 6E). In light of the overall strong conservation of chromatin assembly mechanisms, it will be interesting to see if CHD1 has similar roles in the preservation of healthy lifespan in the mammalian system. Evidence for this comes from a recent study showing that *Chd1* expression in the mouse liver is positively correlated with lifespan (i.e., *Chd1* expression was found to decrease with age), and *Chd1* knockdown upregulated genes with negative correlation to lifespan (Green et al., 2017).

### MRM-HR mass spectrometry for histone H3.3 quantification

Quantification of H3 and its variants is notoriously challenging due to their similar sequences and extensive posttranslational modifications. Here, we used an MRM-HR approach to achieve precise and reproducible quantification of the relative abundance of H3.3 in protein samples from a critically limited source, *Drosophila* fly heads. Targeted proteomics assays, such as MRM (Peterson et al., 2012; Schilling et al., 2015), are less dependent on target protein abundance than data-independent acquisition (DIA; also termed SWATH) methods (Gillet et al., 2012). However, similar to DIA/SWATH, they obviate limitations of information-dependent (IDA) approaches, such as an inherent bias toward abundant peptides and lack of reproducibility. Furthermore, the use of pepsin for protein digestion allowed us to precisely distinguish between H3.3 and H3.1, which represents a major improvement over typical tryptic digestion (El Kennani et al., 2018). We were able to achieve highly reproducible quantification on nanograms of H3 within a crude sample, thereby significantly improving sensitivity compared to an HPLC-based method (McKittrick et al., 2004) that required micrograms of pure H3. Our method greatly improves quantitative analysis of the histone variant H3.3 and should be applicable in diverse eukaryotic systems.

## STAR★METHODS

### RESOURCE AVAILABILITY

**Lead contact**—Further information and requests for resources and reagents should be directed to and will be fulfilled by the lead contact, Dr. Alexandra Lusser, Institute of Molecular Biology, Biocenter, Medical University of Innsbruck, Austria (Alexandra.lusser@i-med.ac.at).

**Materials availability**—Fly strains,  $w^{1118}$ ;  $Chd1^1/Df(2L)Exel^{7014}$ ;  $P\{w^+, elav-Gal4\}/+$ ,  $w^{1118}$ ;  $Chd1^1 P\{w^+, UAS-Chd1\}/Df(2L)Exel^{7014}$ ;  $P\{w^+, elav-Gal4\}/+$  and  $w^{1118}$ ;  $Chd1$ ,  $UAS-sNPF/Df(2L)Exel^{7014}$ ;  $P\{w^+, elav-Gal4\}/UAS-sNPF$  generated in this study will be made available on request. Transfer may require completion of material transfer agreement.

#### Data and code availability

- RNA-seq data have been deposited at the Gene Expression Omnibus repository GEO: GSE146392 and are publicly available as of the date of publication. Raw data ATAC-seq have been deposited at Sequence Read Archive SRA: PRJNA730408. Accession numbers are listed in the Key Resources Table.
- Primer sequences, original western blot images and microscopy data reported in this study will be shared by the lead contact upon request.
- All original code is available in this paper's supplemental information.
- Any additional information required to reanalyze the data reported in this paper is available from the lead contact upon request.

## EXPERIMENTAL MODEL AND SUBJECT DETAILS

**Drosophila strains**—Flies used in the current study were kept at 25°C and 60% humidity in a 12/12 h light/dark cycle in batches of 20 flies on sugar-cornmeal media as described previously (Sebald et al., 2016). Unless otherwise noted, all mutations and transgenes were studied in a  $w^{1118}$  background. *Chd1*-deficient flies (termed  $Chd1^{-/-}$ ) and  $Chd1^{WT/WT}$  flies were generated as described in Konev et al. (2007) and Morettini et al. (2011). For brain-specific expression of *Chd1*, the  $Df(2L)Exel^{7014}$  chromosome was recombined with a *UAS-Chd1* transgene (Konev et al., 2007) by standard procedures. Crosses with the *elav-Gal4* driver line (Bloomington stock center, #8760) were performed for pan-neuronal expression of the transgene in a *Chd1*-negative background. Likewise, *UAS-sNPF* transgene (Lee et al., 2004) and *elav-Gal4* driver were crossed into the  $Chd1^{-/-}$  background. To examine genetic interaction between *Chd1* and *Hira*,  $ssm^{185b}$  flies (Loppin et al., 2000) were crossed to  $Df(2L)Exel^{7014}/CyO$  and  $Chd1^1/CyO$  flies followed by *inter se* crosses. Details about all lines used in this study are shown in Table 1.

## METHOD DETAILS

**Enzymes, chemicals and reagents**—Chemical reagents used in the study were purchased from Acros Organics (New Jersey, USA), Bartlet GmbH (Graz, Austria), Invitrogen (Waltham, USA), Merck (Darmstadt, Germany), Promega (Madison, USA), Sigma Aldrich (St. Louis, USA), Roth (Karlsruhe, Germany), Roche (Basel, Switzerland) and Thermo Fisher Scientific Inc (Waltham, USA). For the in-gel peptide digestion, all reagents were LC-MS grade and purchased from Fisher Scientific, Alfa Aesar and/or Sigma Aldrich. LC separation was performed with trapping and analytical columns from Phenomenex (USA). ATAC-seq samples were prepared using the Tn5 transposase from Illumina (San Diego, USA),

DNA and RNA modifying enzymes were from New England Biolabs (Massachusetts, USA), peptidases were bought from Promega (USA) and metabolically active enzymes were purchased from Sigma Aldrich (St. Louis, USA).

Glucose (HK) Assay Kit and the Serum Triglyceride Determination Kit were bought from Sigma Aldrich (St. Louis, USA). Antibodies were from Sigma Aldrich (USA) or a kind gift from Jessica Tyler.

### MRM-HR mass spectrometry for quantification of H3.3

**Core histone preparation**—Embryos: Wild-type (Oregon R) embryos were collected 0-12 h after egg deposition and chromatin-associated histones were purified to near homogeneity as described (Fyodorov and Levenstein, 2002) and separated by 18% SDS-PAGE (Figure S1).

Whole adult flies: 10 wild-type (Oregon R) flies were immobilized by CO<sub>2</sub>. Chromatin-associated histones were isolated as described (Shechter et al., 2007) with minor modifications. Briefly, flies were homogenized using a RotoDouncer in 0.4 mL Lysis Buffer (15 mM NaCl, 10 mM HEPES-KOH pH 7.6, 2 mM EDTA) containing 0.5% NP-40 and 0.3 M sucrose. The homogenate was loaded onto a discontinuous sucrose gradient (0.4 mL Lysis Buffer containing 0.8 M sucrose and 0.4 mL Lysis Buffer containing 1 M sucrose) in a 1.5 mL Eppendorf tube and centrifuged for 20 min at 4°C at 480 *g*. Diploid nuclei fractionated as translucent band of disperse material in the center of the middle gradient layer (verified by staining with 0.1 µg/mL propidium iodide). The nuclear fraction (< 0.2 mL) was collected, diluted to 0.4 mL with Lysis Buffer, homogenized by a RotoDounce and reloaded onto a discontinuous sucrose gradient as above. The gradient was centrifuged for 10 min at 4°C at 4,300 *g*. The nuclei pellet at the bottom of the gradient was resuspended in 0.5 mL Extraction Buffer (0.5 M NaCl, 10 mM HEPES-KOH pH 7.6, 5 mM MgCl<sub>2</sub>) and incubated at 0°C for 20 min with occasional vortexing. 0.5 M NaCl was included to deplete the non-nucleosomal histone fraction of the nuclei. Nuclei were pelleted (10 min at 16,000 *g*) and extracted with 100 µL 0.4 N H<sub>2</sub>SO<sub>4</sub> overnight at 4°C. After centrifugation (10 min at 16,000 *g*) the supernatant was precipitated with 600 µL cold (-20°C) acetone for 2 h at -20°C and centrifuged at 16,000 *g* for 10 min. The pellet was immediately resuspended in 20 µL 2x Laemmli sample buffer, neutralized with 1 µL 2 M Tris base, boiled and loaded on a 18% SDS-PAGE gel (Figure S1).

Adult fly heads: 20-day-old female flies (*Chd1*<sup>-/-</sup>, *Chd1*<sup>WT/WT</sup>, *Chd1*<sup>elav</sup>) were collected and snap-frozen in liquid nitrogen. Frozen flies were decapitated by vigorous shaking, and heads were separated by passing through a metal sieve. Approximately 65 frozen heads each were distributed to three individual samples, pulverized by Covaris CryoPREP® Dry Impactor and further processed in parallel. The frozen powder was suspended in 0.5 mL Homogenization Buffer (10 mM Tris-HCl pH 8.0, 0.1 mM EDTA, 0.5 M NaCl), homogenized by a RotoDounce and centrifuged at 16,000 *g* for 2 min. The supernatant was discarded and homogenization was repeated once as above. The nuclear pellet was suspended in 0.5 mL H<sub>2</sub>O by douncing, trichloroacetic acid (TCA) was added to a final concentration of 20% with continuous vortexing and precipitation was done over a 30 min incubation period on ice to precipitate non-histone proteins. After centrifugation at 16,000

*g* for 15 min at 4°C, the chromatin pellet was dissolved in 0.4 mL 0.2 N H<sub>2</sub>SO<sub>4</sub> using a RotoDounce and the sample was subjected to sonication in a Bioruptor instrument with 30 cycles of 30 s ON, 30 s OFF. Subsequently, acid extraction was continued over-night at 4°C. Extracts were centrifuged at 16,000 *g* for 30 min at 4°C, and histones were precipitated from the supernatant by drop-wise addition of 198 µL TCA (final concentration 33%) with continuous vortexing, 30 min incubation on ice and centrifugation at 16,000 *g* for 30 min at 4°C. The histone pellet was washed twice with ice-cold acetone (16,000 *g*, 30 min 4°C), dissolved in 20 µL 2x Laemmli sample buffer, boiled and loaded onto a 15% SDS-PAGE gel (Figure S1).

**In-gel digestion with pepsin**—Histone preparations were separated by SDS-PAGE, stained with Coomassie Blue, and H3 protein bands were excised. The gel slices were transferred to 1.5 mL Eppendorf tubes, gently crushed with a RotoDounce pestle, destained with 50% methanol and then with 25 mM ammonium bicarbonate (ABC) in 50% acetonitrile (ACN). The proteins were either reduced by 10 mM dithiothreitol (DTT) for 1 h at 37°C and alkylated with 30 mM iodoacetamide (IAA) for 45 min at room temperature in the dark (embryonic histones) or left non-alkylated (embryonic, adult and head samples). The gel fragments were washed with 25 mM ABC in 50% ACN, dehydrated with 100% ACN, dried in a SpeedVac, rehydrated by addition of 50 µL 40 mM HCl and digested with 0.1-1 µg pepsin (Promega) overnight at 37°C. The peptides were extracted once with 50 µL water and once with 100 µL 25 mM ABC in 50% ACN, all extracts were combined, dried in a SpeedVac and resuspended in 25-500 µL Sample Buffer (0.1% formic acid, FA in 1% ACN). Other peptidases (trypsin, LysargiNase, ArgC and LysN) were also evaluated for their utility for MRM-HR analyses of H3.1 and H3.3 (*data not shown*) but were rejected in favor of pepsin. All reagents were LC-MS grade (Fisher Scientific, Alfa Aesar and/or Sigma Aldrich).

**LC-MS/MS acquisitions**—LC-MS/MS analyses were performed on a TripleTOF 5600+ mass spectrometer (AB SCIEX) coupled with M5 MicroLC system (AB SCIEX/Eksigent) and PAL3 autosampler. LC separation was performed in atrap-elute configuration, which consists of a trapping column (LUNA C18(2), 100 Å, 5 µm, 20 × 0.3 mm cartridge, Phenomenex) and an analytical column (LUNA Omega Polar C18, 100 Å, 3 µm, 150 × 0.3 mm column, Phenomenex). The mobile phase consisted of water with 0.1% FA (phase A) and 100% ACN containing 0.1% FA (phase B). 20 ng to 5 µg total protein was injected for each acquisition. Peptides in Sample Buffer were injected into a 50-µL sample loop, trapped and cleaned on the trapping column with 3% mobile phase B at a flow rate of 25 µL/min for 4 min before being separated on the analytical column with a gradient elution at a flow rate of 5 µL/min. The gradient was set as follows: 0 to 39 min: 3% to 20% phase B, 39 to 50 min: 20% to 40% phase B, 50 to 53 min: 40% to 80% phase B, 53 to 55 min: 80% phase B, 55 to 56 min: 80% to 3% phase B, and 56 to 60 min at 3% phase B. All acquisitions were separated by a blank injection to prevent sample carryover. The mass spectrometer was operated in positive ion mode with EIS voltage at 5,200 V, Source Gas 1 at 30 psi, Source Gas 2 at 20 psi, Curtain Gas at 25 psi and source temperature at 200°C.

**Information-Dependent Acquisition (IDA) and data analysis**—To generate the reference spectral library for MRM-HR data analyses, IDA was performed for several samples of up to 5 µg purified embryonic H3 per injection. The IDA method was set up with a 250-ms TOF-MS scan from 300 to 1250 Da, followed by an MS/MS scan in a high sensitivity mode from 100 to 1500 Da of the top 30 precursor ions above 100 cps threshold (100 ms accumulation time, 100 ppm mass tolerance, rolling collision energy and dynamic accumulation). Each sample was acquired separately for charge states ( $z$ ) from +2 to +5 and from +1 to +2. IDA data files were searched using ProteinPilot (version 5.0.2, ABSciex) with a default setting for purified histones, gel-based ID against a protein sequence database. The *Drosophila* proteome FASTA file with 21,970 protein entries downloaded from UniProt on 3/21/2020 (UP000000803) was used as a reference for the search. Pepsin was used as the protease setting. Up to two missed cleavage sites were allowed. Mass tolerance for precursor and fragment ions was set to 100 ppm. A false discovery rate (FDR) of 1% was used as the cutoff for peptide identification.

Because none of the eight major 7-10 amino acid long peptides overlapping H3.1/H3.3 residues 87-90 that were identified (Table S1, sequences in black) included the cysteine at position 110, their spectra were identical between IAA-alkylated and non-alkylated samples. Thus, DTT-mediated reduction and IAA-mediated carbamylation was omitted for all subsequent MRM-HR acquisitions. Since IDA did not detect all eleven possible 7-10 amino-acid-long peptides spanning from the N-terminal R83 of H3.1 and H3.3, three “hypothetical” peptides were added to the list of MRM-HR target peptides as a control (Table S1, sequences in red).

**MRM-HR acquisition and data analysis**—For MRM-HR acquisition to quantify H3.1/H3.3-specific target peptides based on IDA results (Table S1) one 200-ms TOF-MS scan from 300 to 1250 Da was performed, followed by MS/MS scans from 100 to 1500 Da (100-ms accumulation time, 100 ppm mass tolerance, +2 to +5  $z$ , 2,000,000 cps intensity threshold, 11 maximum candidate ions to monitor per cycle, rolling collision energy) and 11 included precursors at indicated retention times, with a 300 s acquisition window. The intensity threshold of the targeted precursors in the inclusion list was set to 0 cps. Data analysis was carried out with Skyline (version 20.1.0.155) by automatically detecting and matching the MS/MS chromatographic peaks against the spectral library generated from IDA searches. Three “hypothetical” peptide precursors and their predicted product ions were manually inserted in the Skyline spectral library. The MS and MS/MS filtering were both set as “TOF mass analyzer” with the resolution power of 30,000 and 15,000, respectively, while the “Targeted” acquisition method was defined in the MS/MS filtering. Peak selections were checked manually after the automated matches. Although the majority of the peaks (> 95%) were called correctly by Skyline, rarely, the peak boundaries had to be manually adjusted to cover completely and exactly the peak of the dominant (rank 1) product ion. Since the vast majority of MS/MS signal originated from eight IDA-detected peptides, whereas the three hypothetical peptides contributed little to quantitation, respective spectra were acquired in all subsequent MRM-HR experiments but ignored for the purpose of protein quantification. Peptides were then quantified automatically by Skyline based on the extracted ion chromatogram (XIC) areas for the major precursor ion. Peak areas for H3.1-

or H3.3-specific peptides were added together to produce a measure of the total respective protein. Relative H3.3 representation was calculated as  $H3.3/(H3.1 + H3.3)$  for each sample/acquisition. Mean values and standard deviations were calculated for each experimental condition or type of sample. *p-values* between different experimental conditions were calculated by two-tailed Mann-Whitney test. The injected H3 amounts for the different samples were as follows: Embryonic H3 = 300, 80 and 20 ng (> 99% purity); crude preparation of total flies, H3 > 20 ng (~25% purity); crude preparation of fly heads, H3 > 20 ng (~50% purity).

### Western Blot

Frozen female flies (1 d, 10 d) were decapitated by vigorous shaking, and heads were separated by passing through a metal sieve. Approximately 85-100 frozen heads were pulverized by Covaris CryoPREP® Dry Impactor, the powder was suspended in 100  $\mu$ L 1x LSB (0.0625 M Tris; 2% SDS, 10% glycerol, 5% 2-mercapto-ethanol) and sonicated in a Bioruptor instrument for 30 cycles of 30 s ON, 30 s OFF at 4°C. Extracts were centrifuged at 16,000 *g* for 20 min at RT, the supernatant was transferred to a new tube avoiding the lipid layer on top and centrifugation was repeated twice. The remaining supernatant was heated at 95°C for 5 minutes, loaded onto 12% or 8% SDS-PAGE gels and blotted to nitrocellulose membrane. Membranes were blocked in 5% milk/PBS and incubated overnight at 4°C with primary antibodies followed by washing in PBS and incubation with HRP-coupled secondary antibody (Sigma, 1:10,000). Signal development was done by incubation with ECL (GE Healthcare) followed by detection using a Fusion-SL 3500-WL system (PeqLab) and Fusion software (v15.17). The following antibodies were used: rabbit  $\alpha$ -dmXNP15879 (1:1,000; [Emelyanov et al., 2010]); rabbit  $\alpha$ -dmHIRA (1:5,000), rabbit  $\alpha$ -dmASF1 (1:20,000; kind gift of Jessica Tyler); mouse  $\alpha$ -tubulin (1:10,000; Sigma T5168).

### Reverse transcription real-time PCR (RT-qPCR)

For RT-qPCR analyses virgin females of the genotypes indicated in Figure 6 were used. Flies were aged in food vials (at 20 flies each) until 4, 7 or 14 days old and subsequently pooled. Three batches of 100 flies were randomly collected from the pools and processed for further analysis. Briefly, flies were snap frozen, decapitated by vigorous shaking of the frozen carcasses and head and abdominal tissues were separated by passing through a sieve. The frozen tissues were pulverized by Covaris CryoPREP® Dry Impactor, total RNA was extracted using TRI Reagent® (Sigma Aldrich) followed by DNase I digestion and cDNA synthesis. qPCR was performed in triplicate using Luna® Universal qPCR Master Mix (NEB) with 25 ng cDNA and 0.4  $\mu$ M of target-specific primers in a QuantStudio 3 instrument (Thermo Fisher). Primer sequences are available upon request.  $2^{-C_t}$  values were calculated and statistical analysis was done by unpaired Student's *t* test (Graphpad Prism 8.2.1).

### RNA-seq

Total RNA was extracted as described above from heads of virgin females of the following genotypes: *Chd1*<sup>-/-</sup>, *Chd1*<sup>WT/WT</sup>, *Chd1*<sup>-/-</sup>; *elav*-Gal4 (driver control), *Chd1*<sup>-/-</sup>; *UAS-Chd1* (transgene control) and *Chd1*<sup>elav</sup> flies (see also Table 1). Crosses for all genotypes were handled side-by-side. Flies were kept in separate food vials (20 each) until 10 days old

and subsequently pooled. Three batches of 200 flies each were randomly collected from the pools and processed for further analysis. mRNA enrichment, library preparation and sequencing were done by BGI Genomics Co., Ltd. About 6.35 Gb paired-end 100 nt reads per sample were generated.

### ATAC-seq

Tagmentation and library preparation for ATAC-seq were performed essentially as described by Davie et al. (2018) with minor alterations. Briefly, two brains each of *Chd1*<sup>-/-</sup>, *Chd1*<sup>wr/Wr</sup> and *H3.3 KO* female flies were dissected, washed in ice cold PBS and transferred to Lysis Buffer (10 mM Tris-HCl, pH 7.4, 10 mM NaCl, 3 mM MgCl<sub>2</sub>, 0.1% Igepal CA-630, 1x Protease Inhibitor Cocktail (Roche)). Brains were disrupted by vigorous pipetting and by grinding with a plastic pestle. After centrifugation at 800 *g* for 10 min, 50  $\mu$ L ATAC-seq reaction mix (2.5  $\mu$ L Nextera Tn5 (Illumina), 25  $\mu$ L Nextera TD Buffer (Illumina), 22.5  $\mu$ L a.d.) were added to the chromatin pellet and incubated for 30 min at 37°C. The experiment was performed in duplicates for each genotype. Transposed DNA was purified using the NEB Monarch DNA purification kit and subjected to library amplification PCR using Q5 polymerase (NEB), the forward primer Ad1\_noMX and one of the reverse primers Ad2.1-Ad2.3 or Ad2.7-Ad2.12 from Buenrostro et al. (2013) for each sample with the following PCR conditions: 72°C for 1 min, 98°C for 30 s, 12 cycles of 98°C for 10 s, 63°C for 30 s, 72°C for 1 min. Libraries were purified by NEB PCR purification kit and submitted to 150 bp paired-end sequencing on a Novaseq instrument (Zymo Research).

### Lifespan analysis

Virgin female flies were reared in batches of 20 under standard humidity and light conditions on standard food (110 g/L refined sugar, 52 g/L cornmeal, 27.5 g/L brewer's yeast, 4 g/L agar, 2.4 g/L tegosept dissolved in ethanol). Flies were transferred to fresh vials every three days. For dietary intervention experiments, standard food was either supplemented with 0.2 mM rapamycin (Sigma Aldrich) or the sugar concentration was changed to 342 g/L sugar ("high sugar") and 51 g/L sugar ("low sugar"), respectively (Figure S9). Viability was monitored daily and dead flies were removed. Survival rates are expressed as percentage of living flies at each given time point.

### Consumption analysis

**Body weight measurement**—For determination of wet weight, virgin female flies, aged 7 days, were lightly anesthetized with CO<sub>2</sub> and weighed in batches of ten (5 batches). The flies were then lyophilized overnight and weighed again to obtain the dry weight.

**A<sub>630</sub> colorimetric assay**—Virgin female flies were selected and aged for 4 or 14 days under standard conditions and standard food. To determine food intake, flies were transferred to food vials containing filter discs soaked in blue food coloring (100 mg/ml E133 brilliant blue food coloring in 0.05% sucrose solution). After 30 min at 25°C, the vials were frozen in liquid nitrogen, and 10 frozen flies were transferred to an Eppendorf tube for homogenization in TES buffer (1 mM EDTA, 10 mM Tris-HCl pH 7.5, 100 mM NaCl, 0.1% Triton® X-100). Homogenates were centrifuged at 14,000 *g* and supernatants were measured in a spectrophotometer at 630 nm. Supernatants from flies fed with non-colored

food were used as a reference. Independent feeding experiments were performed at the exact same time of the day. Consumption was scored as absorption  $A_{630}$  per fly.

**CAFE assay**—4-, 7- and 14-day-old virgin female flies were used in a capillary feeder (CAFE) assay as described (Deshpande et al., 2014). To this end, starved flies (24 hours on 1%PBS/10% agarose media) were transferred from the starvation vials into the CAFE containers without the use of anesthesia and tested individually. Consumption was measured by monitoring the descent of the meniscus in the capillaries at 15 min, 30 min, 1 h and 2 h. Mean values of absolute consumption per fly were calculated and plotted.

### Metabolic profiling

**Metabolome analysis by UPLC-MS**—Whole fly extracts were prepared by methanol extraction from 4- and 14-d-old male or female flies of the indicated genotype in 1-5 replicates (pools of 15 flies) and metabolome analysis was performed by UPLC-MS as described previously (Cázares-García et al., 2017). Amino acid profiles were determined by the method of Bidlingmeyer et al. (1984). Chromatography was performed on an Agilent 1200 system, using a Pico-Tag column (3.9x150 mm) and a detection wavelength of 254 nm. The results were normalized to the total amino acid concentrations to compensate for errors due to low sample quantities.

**Circulating and storage metabolites**—Circulating metabolites glucose and trehalose were measured in hemolymph of virgin female 4-, 7- and 14-day-old flies (pools of 40-50 flies). To this end, flies were washed by submersion in ice-cold 1xPBS in a 0.5 mL tube perforated at the bottom with a 25G needle. The tube was placed into a 1.5 mL tube and centrifuged at 5000 rpm, 4°C for 5 min. The flies were then pricked into the thorax with a 30G needle and transferred into a fresh perforated 0.5 mL tube. Centrifugation was repeated and the collected hemolymph in the bottom tube was snap-frozen and stored at  $-80^{\circ}\text{C}$ . Whole fly extracts (pools of 5 flies) were prepared for the measurement of glycogen and triacylglyceride (TAG). Briefly, flies were washed with ice-cold 1xPBS as described above and snap-frozen in liquid nitrogen. Subsequently, 0.1 mL of ice-cold 1xPBS-T was added and the flies were homogenized with a small plastic pestle. Ten  $\mu\text{L}$  of the homogenate was removed, centrifuged 3 min at maximum speed and the supernatant used for protein concentration measurement by Bradford assay. The rest of the homogenate was heated for ten minutes at  $70^{\circ}\text{C}$ , centrifuged at maximum speed for 3 min at  $4^{\circ}\text{C}$ , and the supernatant was stored at  $-80^{\circ}\text{C}$  or used immediately. Glucose was determined using the Glucose (HK) Assay Kit (Sigma Aldrich) according to the kit's instructions. For determining trehalose and glycogen levels, hemolymph or whole fly extracts were heat-inactivated at  $70^{\circ}\text{C}$  for 5 min before treatment with porcine trehalase (Sigma Aldrich) O/N at  $37^{\circ}\text{C}$  to release glucose and with amyloglycosidase (Sigma Aldrich), respectively, to digest glycogen into glucose. The resulting glucose was measured as above. To determine TAG levels in whole fly extracts, Serum Triglyceride Determination Kit (Sigma Aldrich) was used according to manufacturer's instructions. Metabolites from whole cell extracts were normalized to total protein concentration.

**Cardiolipin analysis by HPLC-MS/MS**—Whole fly extracts were prepared by methanol extraction from 4- and 14-day-old male or female flies of the indicated genotype in 5 replicates (20 flies/replicate) and cardiolipins were analyzed by LC-MS/MS exactly as described previously (Oemer et al., 2018). The molecular cardiolipin profiles were used to compute the average number of side chain carbon atoms and double bonds in each group.

## QUANTIFICATION AND STATISTICAL ANALYSIS

**MRM-HR mass spectrometry**—IDA data files were searched using ProteinPilot (version 5.0.2, ABSciex) with a default setting for purified histones, gel-based ID against a protein sequence database. The *Drosophila* proteome FASTA file with 21,970 protein entries downloaded from UniProt on 3/21/2020 (UP000000803) was used as a reference for the search. MRM-HR Data analysis was carried out with Skyline (version 20.1.0.155). Mean values and standard deviations were calculated for each experimental condition or type of sample. *p-values* between different experimental conditions were calculated by two-tailed Mann-Whitney test. Experiments were performed with technical and/or biological replicates of two independent crossings as indicated at the representing figure.

**Western blot**—Experiments were replicated three times and band intensities were quantified by ImageJ (RRID:SCR\_003070) software. Statistical analysis was performed by multiple unpaired t test.

**Reverse transcription real-time PCR (RT-qPCR)**—Real time qPCR data were analyzed by QuantStudio 3 System. Experiments were replicated at least three times with technical replicates each time as indicated at the representing figure. Raw data was extracted from QuantStudio 3 System (Thermo Fisher) and processed in Excel and Graphpad Prism 8.2.1.. Statistical analysis was performed by unpaired t test and method and significance are indicated in the figure or figure legend.

**RNA-seq**—Transcript abundance was quantified using Salmon (Patro et al., 2017) and the *D. melanogaster* RefSeq assembly GCF\_000001215.4\_Release\_6\_plus\_ISO1\_MT transcriptome downloaded from NCBI. For further analysis, Salmon output was imported into R (version 3.6.1, <https://www.r-project.org>) using the Bioconductor (Huber et al., 2015) R package tximport (Soneson et al., 2015). Threshold for genes regarded as being expressed was set to TPM > 1 (mean of three replicates of any condition as calculated by Salmon). Differential expression calling was performed with DESeq2 (Love et al., 2014). For visualization by volcano plots, the l2fc value from DESeq2 was shrunk using the apeglm algorithm (Zhu et al., 2019). Genes were regarded as being differentially expressed when meeting the criteria  $l2fc \geq 1$  and adjusted p value < 0.05. Genes upregulated in *Chd1*<sup>-/-</sup> versus *Chd1*<sup>WT/WT</sup> and *Chd1*<sup>-/-</sup> versus *Chd1*<sup>elav</sup> were submitted to gene ontology enrichment (biological process) analysis using DAVID v6.8 (Huang et al., 2009). Functional categories with an adjusted p value < 0.05 (Benjamini) were defined as significantly enriched. Heatmaps were generated using the R package pheatmap (Kolde, 2019). Generation of tables and plots was performed using the R packages dplyr (Wickham et al., 2020), ggplot2 (Wickham, 2016), and eulerr (Larsson, 2019). RNA-seq data are available at the Gene Expression Omnibus repository GEO: GSE146392.

**ATAC-seq**—ATAC-seq reads were processed using the nf-core/atacseq v1.2.1 pipeline (<https://github.com/nf-core/atacseq>) (Ewels et al., 2020). The workflow includes quality control of raw reads by FastQC v0.11.9 and adaptor trimming by Trim Galore! v0.6.4. Reads were mapped to the BDGP6 reference genome by BWA v0.7.17-r1188 (Li and Durbin, 2009), and SAMtools v1.10 (Li et al., 2009) was used to remove reads from mitochondrial DNA and blacklisted regions as well as other low-quality reads. Peaks were called by MACS2 v2.2.7.1 (parameters: *-f BAMPE -g 1.2e8-keep-dup all-nomodel*) (Zhang et al., 2008). HOMER v4.11 (Heinz et al., 2010) was used for peak annotation. Reads in consensus peaks were counted with featureCounts v2.0.1 (Liao et al., 2014), and DESeq2 v1.26.0 (Love et al., 2014) was used for differential accessibility analysis and PCA. Normalized peak intensities ( $cpm_{(i)}$ ) were calculated as read count in peaks/total mapped read count  $\times 10^6$ . To remove extreme outliers, a 99% quantile capping was applied, and retained peak intensities were analyzed for statistically significant differences by Kruskal-Wallis test. Heatmaps displaying normalized read densities of ATAC-seq samples were generated with the computeMatrix and plotHeatmap modules of the deepTools suite v3.5.1 (Ramírez et al., 2014) in “reference-point” mode. K-means clusters (k = 4) obtained by the plotHeatmap function applied to the *Chd1*<sup>-/-</sup> condition were then recycled for all conditions. Raw data have been deposited at Sequence Read Archive SRA: PRJNA730408.

**Lifespan analysis**—Raw data was processed in Excel and Prism (Graphpad Prism 8.2.1.). At least three independent experiments (100-200 flies each) were performed for each condition unless stated otherwise (Figure 5E) and statistical analysis of survival curves was performed by Mantel-Cox test (Graphpad Prism 8.2.1).

**Consumption analysis**—Experiments were performed with at least three biological replicates (definite numbers are stated in the respective figure legends).

**Body weight measurement:** Mean weight  $\pm$  SEM per fly per replicate was calculated and statistical analysis was done by unpaired t test (Graphpad Prism 8.2.1).

**A<sub>630</sub> colorimetric assay:** Three independent experiments with 5 batches of 10 flies for each age group and genotype were performed. Results were analyzed for statistical significance by unpaired t test (Graphpad Prism 8.2.1).

**CAFE assay:** Statistical analysis of the mean values of absolute consumption was performed by 3-way ANOVA (genotype  $\times$  age  $\times$  measurement time point). Six batches of 20 flies were tested for each genotype and age.

### Metabolic profiling

**Metabolome analysis by UPLC-MS & Cardiolipin analysis by HPLC-MS/MS:** UPLC-MS and HPLC-MS/MS acquired data was analyzed and visualized using R (version 3.6.1, <https://www.r-project.org>) as described in Cázarez-García et al. (2017) and Oemer et al. (2018). Experiments were performed with 1-5 replicates for each genotype, age group and sex. Definite numbers are indicated in the respective figure legends.

**Circulating and storage metabolites:** In all experiments, technical triplicates were measured and three independent experiments were performed. 2-way ANOVA and Tukey post hoc test (Graphpad Prism 8.2.1) were performed for statistical analysis.

**Significance**—\*  $p < 0.05$ /\*\*  $p < 0.01$ /\*\*\*  $p < 0.001$ \*\*\*\*  $p < 0.0001$ /ns = not significant.

The statistical details of experiments are presented in the relevant figure legends. A  $p$  value of  $< 0.05$  was considered significant.

## Supplementary Material

Refer to Web version on PubMed Central for supplementary material.

## ACKNOWLEDGMENTS

We thank Konrad Basler, Kweon Yu and Benjamin Loppin for the gift of fly strains. We appreciate the help with methods and techniques by Gabriele Salcher-Scheran, Alexandra Wille, Carla Margulies, Sina Kunz, Dominik Brück, and Nico Wahl, and we are grateful to Peter Loidl and Simone Sidoli for critically reading the manuscript and helpful comments. Research on this project was funded by the Austrian Science Fund (FWF) (P31377-B30 to A.L.), the NIH (GM074233 to D.V.F.), and the Consejo Nacional de Ciencia y Tecnología (CONACyT) Mexico (FRONTERAS 2015-2/814 and CONACyT-DFG 2016/277850 to R.W. and D.C.G. [Scholarship]).

## REFERENCES

- Alén C, Kent NA, Jones HS, O'Sullivan J, Aranda A, and Proudfoot NJ (2002). A role for chromatin remodeling in transcriptional termination by RNA polymerase II. *Mol. Cell* 10, 1441–1452. [PubMed: 12504018]
- Antikainen H, Driscoll M, Haspel G, and Dobrowolski R (2017). TOR-mediated regulation of metabolism in aging. *Aging Cell* 16, 1219–1233. [PubMed: 28971552]
- Augello MA, Liu D, Deonaraine LD, Robinson BD, Huang D, Stelloo S, Blattner M, Doane AS, Wong EWP, Chen Y, et al. (2019). CHD1 Loss Alters AR Binding at Lineage-Specific Enhancers and Modulates Distinct Transcriptional Programs to Drive Prostate Tumorigenesis. *Cancer Cell* 35, 603–617.e8. [PubMed: 30930119]
- Bano D, Piazzesi A, Salomoni P, and Nicotera P (2017). The histone variant H3.3 claims its place in the crowded scene of epigenetics. *Aging (Albany NY)* 9, 602–614. [PubMed: 28284043]
- Bidlingmeyer BA, Cohen SA, and Tarvin TL (1984). Rapid analysis of amino acids using pre-column derivatization. *J. Chromatogr. A* 336, 93–104.
- Bonnefoy E, Orsi GA, Couble P, and Loppin B (2007). The essential role of *Drosophila* HIRA for de novo assembly of paternal chromatin at fertilization. *PLoS Genet.* 3, 1991–2006. [PubMed: 17967064]
- Broughton SJ, Piper MDW, Ikeya T, Bass TM, Jacobson J, Driege Y, Martinez P, Hafen E, Withers DJ, Leivers SJ, and Partridge L (2005). Longer lifespan, altered metabolism, and stress resistance in *Drosophila* from ablation of cells making insulin-like ligands. *Proc. Natl. Acad. Sci. USA* 102, 3105–3110. [PubMed: 15708981]
- Buenrostro JD, Giresi PG, Zaba LC, Chang HY, and Greenleaf WJ (2013). Transposition of native chromatin for fast and sensitive epigenomic profiling of open chromatin, DNA-binding proteins and nucleosome position. *Nat. Methods* 10, 1213–1218. [PubMed: 24097267]
- Cázaréz-García D, Ramírez Loustalot-Laclette M, Ann Markow T, and Winkler R (2017). Lipidomic profiles of *Drosophila melanogaster* and cactophilic fly species: models of human metabolic diseases. *Integr. Biol* 9, 885–891.
- Clapier CR, and Cairns BR (2009). The biology of chromatin remodeling complexes. *Annu. Rev. Biochem* 78, 273–304. [PubMed: 19355820]

- Clark RI, and Walker DW (2018). Role of gut microbiota in aging-related health decline: insights from invertebrate models. *Cell. Mol. Life Sci* 75, 93–101. [PubMed: 29026921]
- Davie K, Janssens J, Koldere D, De Waegeneer M, Pech U, Kreft Ł, Aibar S, Makhzami S, Christiaens V, Bravo González-Blas C, et al. (2018). A Single-Cell Transcriptome Atlas of the Aging *Drosophila* Brain. *Cell* 174, 982–998.e20. [PubMed: 29909982]
- de Dieuleveult M, Yen K, Hmitou I, Depaux A, Boussouar F, Bou Dargham D, Jounier S, Humbertclaude H, Ribierre F, Baulard C, et al. (2016). Genome-wide nucleosome specificity and function of chromatin remodellers in ES cells. *Nature* 530, 113–116. 10.1038/nature16505. [PubMed: 26814966]
- Deshpande SA, Carvalho GB, Amador A, Phillips AM, Hoxha S, Lizotte KJ, and Ja WW (2014). Quantifying *Drosophila* food intake: comparative analysis of current methodology. *Nat. Methods* 11, 535–540. [PubMed: 24681694]
- Drané P, Ouararhni K, Depaux A, Shuaib M, and Hamiche A (2010). The death-associated protein DAXX is a novel histone chaperone involved in the replication-independent deposition of H3.3. *Genes Dev.* 24, 1253–1265. [PubMed: 20504901]
- El Kennani S, Adrait A, Permiakova O, Hesse A-M, Ialy-Radio C, Ferro M, Brun V, Cocquet J, Govin J, and Pflieger D (2018). Systematic quantitative analysis of H2A and H2B variants by targeted proteomics. *Epigenetics Chromatin* 11, 2. [PubMed: 29329550]
- Emelyanov AV, Konev AY, Vershilova E, and Fyodorov DV (2010). Protein complex of *Drosophila* ATRX/XNP and HP1a is required for the formation of pericentric beta-heterochromatin in vivo. *J. Biol. Chem* 285, 15027–15037. [PubMed: 20154359]
- Erkosar B, and Leulier F (2014). Transient adult microbiota, gut homeostasis and longevity: novel insights from the *Drosophila* model. *FEBS Lett.* 588, 4250–4257. [PubMed: 24983497]
- Ewels PA, Peltzer A, Fillinger S, Patel H, Alneberg J, Wilm A, Garcia MU, Di Tommaso P, and Nahnsen S (2020). The nf-core framework for community-curated bioinformatics pipelines. *Nat. Biotechnol* 38, 276–278. [PubMed: 32055031]
- Fei J, Torigoe SE, Brown CR, Khuong MT, Kassavetis GA, Boeger H, and Kadonaga JT (2015). The prenucleosome, a stable conformational isomer of the nucleosome. *Genes Dev.* 29, 2563–2575. [PubMed: 26680301]
- Fontana L, and Partridge L (2015). Promoting health and longevity through diet: from model organisms to humans. *Cell* 161, 106–118. [PubMed: 25815989]
- Franceschi C, Garagnani P, Parini P, Giuliani C, and Santoro A (2018). Inflammaging: a new immune-metabolic viewpoint for age-related diseases. *Nat. Rev. Endocrinol* 14, 576–590. [PubMed: 30046148]
- Fyodorov DV, and Levenstein ME (2002). Chromatin assembly using *Drosophila* systems. *Curr. Protoc. Mol. Biol* Chapter 21, Unit 21.7.27.
- Galenza A, and Foley E (2019). Immunometabolism: Insights from the *Drosophila* model. *Dev. Comp. Immunol* 94, 22–34. [PubMed: 30684503]
- Gaspar-Maia A, Alajem A, Polesso F, Sridharan R, Mason MJ, Heidersbach A, Ramalho-Santos J, McManus MT, Plath K, Meshorer E, and Ramalho-Santos M (2009). Chd1 regulates open chromatin and pluripotency of embryonic stem cells. *Nature* 460, 863–868. [PubMed: 19587682]
- Giannakou ME, and Partridge L (2007). Role of insulin-like signalling in *Drosophila* lifespan. *Trends Biochem. Sci* 32, 180–188. [PubMed: 17412594]
- Gillet LC, Navarro P, Tate S, Röst H, Selevsek N, Reiter L, Bonner R, and Aebersold R (2012). Targeted data extraction of the MS/MS spectra generated by data-independent acquisition: a new concept for consistent and accurate proteome analysis. *Mol. Cell Proteomics* 11, O111.016717.
- Goldberg AD, Banaszynski LA, Noh K-M, Lewis PW, Elsaesser SJ, Stadler S, Dewell S, Law M, Guo X, Li X, et al. (2010). Distinct factors control histone variant H3.3 localization at specific genomic regions. *Cell* 140, 678–691. [PubMed: 20211137]
- Green CD, Huang Y, Dou X, Yang L, Liu Y, and Han JJ (2017). Impact of Dietary Interventions on Noncoding RNA Networks and mRNAs Encoding Chromatin-Related Factors. *Cell Rep.* 18, 2957–2968. [PubMed: 28329687]
- Grover P, Asa JS, and Campos EI (2018). H3-H4 Histone Chaperone Pathways. *Annu. Rev. Genet* 52, 109–130. [PubMed: 30183406]

- Guzman-Ayala M, Sachs M, Koh FM, Onodera C, Bulut-Karslioglu A, Lin C-J, Wong P, Nitta R, Song JS, and Ramalho-Santos M (2015). Chd1 is essential for the high transcriptional output and rapid growth of the mouse epiblast. *Development* 142, 118–127. [PubMed: 25480920]
- Harrison B, Tran TT, Taylor D, Lee S-D, and Min K-J (2010). Effect of rapamycin on lifespan in *Drosophila*. *Geriatr. Gerontol. Int* 10, 110–112. [PubMed: 20102391]
- Heinz S, Benner C, Spann N, Bertolino E, Lin YC, Laslo P, Cheng JX, Murre C, Singh H, and Glass CK (2010). Simple combinations of lineage-determining transcription factors prime cis-regulatory elements required for macrophage and B cell identities. *Mol. Cell* 38, 576–589. [PubMed: 20513432]
- Hennig BP, Bendrin K, Zhou Y, and Fischer T (2012). Chd1 chromatin remodelers maintain nucleosome organization and repress cryptic transcription. *EMBO Rep.* 13, 997–1003. [PubMed: 23032292]
- Hödl M, and Basler K (2009). Transcription in the absence of histone H3.3. *Curr. Biol* 19, 1221–1226. [PubMed: 19523831]
- Huang W, Sherman BT, and Lempicki RA (2009). Systematic and integrative analysis of large gene lists using DAVID bioinformatics resources. *Nat. Protoc* 4, 44–57. [PubMed: 19131956]
- Huber W, Carey VJ, Gentleman R, Anders S, Carlson M, Carvalho BS, Bravo HC, Davis S, Gatto L, Girke T, et al. (2015). Orchestrating high-throughput genomic analysis with Bioconductor. *Nat. Methods* 12, 115–121. [PubMed: 25633503]
- Kolde R (2019). pheatmap: Pretty Heatmaps. <https://cran.r-project.org/web/packages/pheatmap/index.html>.
- Konev AY, Tribus M, Park SY, Podhraski V, Lim CY, Emelyanov AV, Vershilova E, Pirrotta V, Kadonaga JT, Lusser A, and Fyodorov DV (2007). CHD1 motor protein is required for deposition of histone variant H3.3 into chromatin in vivo. *Science* 317, 1087–1090. 10.1126/science.1145339. [PubMed: 17717186]
- Landis GN, Abdueva D, Skvortsov D, Yang J, Rabin BE, Carrick J, Tavaré S, and Tower J (2004). Similar gene expression patterns characterize aging and oxidative stress in *Drosophila melanogaster*. *Proc. Natl. Acad. Sci. USA* 101,7663–7668. [PubMed: 15136717]
- Larsson J (2019). eulerr: Area-Proportional Euler and Venn Diagrams with Ellipses. <https://cran.r-project.org/web/packages/eulerr/index.html>.
- Lee K-A, and Lee W-J (2014). *Drosophila* as a model for intestinal dysbiosis and chronic inflammatory diseases. *Dev. Comp. Immunol* 42, 102–110. [PubMed: 23685204]
- Lee K-S, You K-H, Choo J-K, Han Y-M, and Yu K (2004). *Drosophila* short neuropeptide F regulates food intake and body size. *J. Biol. Chem* 279, 50781–50789. [PubMed: 15385546]
- Lee J-S, Garrett AS, Yen K, Takahashi Y-H, Hu D, Jackson J, Seidel C, Pugh BF, and Shilatifard A (2012). Codependency of H2B monoubiquitination and nucleosome reassembly on Chd1. *Genes Dev.* 26, 914–919. [PubMed: 22549955]
- Lee Y, Park D, and Iyer VR (2017). The ATP-dependent chromatin remodeler Chd1 is recruited by transcription elongation factors and maintains H3K4me3/H3K36me3 domains at actively transcribed and spliced genes. *Nucleic Acids Res.* 45, 7180–7190. [PubMed: 28460001]
- Levendosky RF, Sabantsev A, Deindl S, and Bowman GD (2016). The Chd1 chromatin remodeler shifts hexasomes unidirectionally. *elife* 5, 3302.
- Li H, and Durbin R (2009). Fast and accurate short read alignment with Burrows-Wheeler transform. *Bioinformatics* 25, 1754–1760. [PubMed: 19451168]
- Li H, Handsaker B, Wysoker A, Fennell T, Ruan J, Homer N, Marth G, Abecasis G, and Durbin R; 1000 Genome Project Data Processing Subgroup (2009). The Sequence Alignment/Map format and SAMtools. *Bioinformatics* 25,2078–2079. [PubMed: 19505943]
- Liao Y, Smyth GK, and Shi W (2014). featureCounts: an efficient general purpose program for assigning sequence reads to genomic features. *Bioinformatics* 30, 923–930. [PubMed: 24227677]
- Lin JJ, Lehmann LW, Bonora G, Sridharan R, Vashisht AA, Tran N, Plath K, Wohlschlegel JA, and Carey M (2011). Mediator coordinates PIC assembly with recruitment of CHD1. *Genes Dev.* 25, 2198–2209. [PubMed: 21979373]
- Lin S, Senapati B, and Tsao C-H (2019). Neural basis of hunger-driven behaviour in *Drosophila*. *Open Biol.* 9, 180259. [PubMed: 30914005]

- Loppin B, Docquier M, Bonneton F, and Couble P (2000). The maternal effect mutation sesame affects the formation of the male pronucleus in *Drosophila melanogaster*. *Dev. Biol* 222, 392–404. [PubMed: 10837127]
- Loppin B, Bonnefoy E, Anselme C, Laurençon A, Karr TL, and Couble P (2005). The histone H3.3 chaperone HIRA is essential for chromatin assembly in the male pronucleus. *Nature* 437, 1386–1390. [PubMed: 16251970]
- Love MI, Huber W, and Anders S (2014). Moderated estimation of fold change and dispersion for RNA-seq data with DESeq2. *Genome Biol.* 15, 550. [PubMed: 25516281]
- Lusser A, and Kadonaga JT (2004). Strategies for the reconstitution of chromatin. *Nat. Methods* 1, 19–26. [PubMed: 15789029]
- Lusser A, Urwin DL, and Kadonaga JT (2005). Distinct activities of CHD1 and ACF in ATP-dependent chromatin assembly. *Nat. Struct. Mol. Biol* 12, 160–166. [PubMed: 15643425]
- Martire S, and Banaszynski LA (2020). The roles of histone variants in fine-tuning chromatin organization and function. *Nat. Rev. Mol. Cell Biol* 21, 522–541. [PubMed: 32665685]
- Mattila J, Havula E, Suominen E, Teesalu M, Surakka I, Hynynen R, Kilpinen H, Väänänen J, Hovatta I, Käkälä R, et al. (2015). Mondo-Mlx Mediates Organismal Sugar Sensing through the Gli-Similar Transcription Factor Sugarbabe. *Cell Rep.* 13, 350–364. [PubMed: 26440885]
- McKittrick E, Gafken PR, Ahmad K, and Henikoff S (2004). Histone H3.3 is enriched in covalent modifications associated with active chromatin. *Proc. Natl. Acad. Sci. USA* 101, 1525–1530. [PubMed: 14732680]
- Moretini S, Tribus M, Zeilner A, Sebald J, Campo-Fernandez B, Scheran G, Wörle H, Podhraski V, Fyodorov DV, and Lusser A (2011). The chromodomains of CHD1 are critical for enzymatic activity but less important for chromatin localization. *Nucleic Acids Res.* 39, 3103–3115. [PubMed: 21177652]
- Nässel DR, and Zandawala M (2019). Recent advances in neuropeptide signaling in *Drosophila*, from genes to physiology and behavior. *Prog. Neurobiol* 179, 101607. [PubMed: 30905728]
- Oemer G, Lackner K, Muigg K, Krumschnabel G, Watschinger K, Sailer S, Lindner H, Gnaiger E, Wortmann SB, Werner ER, et al. (2018). Molecular structural diversity of mitochondrial cardiolipins. *Proc. Natl. Acad. Sci. USA* 115, 4158–4163. [PubMed: 29618609]
- Orsi GA, Algazeery A, Meyer RE, Capri M, Sapay-Triomphe LM, Horard B, Gruffat H, Couble P, Ait-Ahmed O, and Loppin B (2013). *Drosophila* Yemanuclein and HIRA cooperate for de novo assembly of H3.3-containing nucleosomes in the male pronucleus. *PLoS Genet.* 9, e1003285. [PubMed: 23408912]
- Patro R, Duggal G, Love MI, Irizarry RA, and Kingsford C (2017). Salmon provides fast and bias-aware quantification of transcript expression. *Nat. Methods* 14, 417–419. [PubMed: 28263959]
- Pchelintsev NA, McBryan T, Rai TS, van Tuyn J, Ray-Gallet D, Almouzni G, and Adams PD (2013). Placing the HIRA histone chaperone complex in the chromatin landscape. *Cell Rep.* 3, 1012–1019. [PubMed: 23602572]
- Peterson AC, Russell JD, Bailey DJ, Westphall MS, and Coon JJ (2012). Parallel reaction monitoring for high resolution and high mass accuracy quantitative, targeted proteomics. *Mol. Cell. Proteomics* 11, 1475–1488. [PubMed: 22865924]
- Petes SJ, and Lis JT (2008). Rapid, transcription-independent loss of nucleosomes over a large chromatin domain at Hsp70 loci. *Cell* 134, 74–84. [PubMed: 18614012]
- Qiu Y, Levendosky RF, Chakravarthy S, Patel A, Bowman GD, and Myong S (2017). The Chd1 Chromatin Remodeler Shifts Nucleosomal DNA Bidirectionally as a Monomer. *Mol. Cell* 68, 76–88.e6. [PubMed: 28943314]
- Quan TK, and Hartzog GA (2010). Histone H3K4 and K36 methylation, Chd1 and Rpd3S oppose the functions of *Saccharomyces cerevisiae* Spt4-Spt5 in transcription. *Genetics* 184, 321–334. [PubMed: 19948887]
- Radman-Livaja M, Quan TK, Valenzuela L, Armstrong JA, van Welsem T, Kim T, Lee LJ, Buratowski S, van Leeuwen F, Rando OJ, and Hartzog GA (2012). A key role for Chd1 in histone H3 dynamics at the 3' ends of long genes in yeast. *PLoS Genet.* 8, e1002811. [PubMed: 22807688]
- Ramírez F, Dündar F, Diehl S, Grüning BA, and Manke T (2014). deep-Tools: a flexible platform for exploring deep-sequencing data. *Nucleic Acids Res.* 42, W187–91. [PubMed: 24799436]

- Rera M, Clark RI, and Walker DW (2012). Intestinal barrier dysfunction links metabolic and inflammatory markers of aging to death in *Drosophila*. *Proc. Natl. Acad. Sci. USA* 109, 21528–21533. [PubMed: 23236133]
- Reyes-DelaTorre A, Pena-Rangel MT, and Riesgo-Escovar JR (2012). Carbohydrate metabolism in *Drosophila*: reliance on the disaccharide trehalose. *Carbohydrates - Comprehensive Studies on Glycobiology and Glycotechnology (InTech)*, pp. 1–22.
- Ribeiro C, and Dickson BJ (2010). Sex peptide receptor and neuronal TOR/S6K signaling modulate nutrient balancing in *Drosophila*. *Curr. Biol* 20,1000–1005. [PubMed: 20471268]
- Rippe K, Schrader A, Riede P, Strohner R, Lehmann E, and Längst G (2007). DNA sequence- and conformation-directed positioning of nucleosomes by chromatin-remodeling complexes. *Proc. Natl. Acad. Sci. USA* 104,15635–15640. [PubMed: 17893337]
- Schilling B, MacLean B, Held JM, Sahu AK, Rardin MJ, Sorensen DJ, Peters T, Wolfe AJ, Hunter CL, MacCoss MJ, and Gibson BW (2015). Multiplexed, Scheduled, High-Resolution Parallel Reaction Monitoring on a Full Scan QqTOF Instrument with Integrated Data-Dependent and Targeted Mass Spectrometric Workflows. *Anal. Chem* 87, 10222–10229. [PubMed: 26398777]
- Schinaman JM, Rana A, Ja WW, Clark RI, and Walker DW (2019). Rapamycin modulates tissue aging and lifespan independently of the gut microbiota in *Drosophila*. *Sci. Rep* 9, 7824. [PubMed: 31127145]
- Sebald J, Morettini S, Podhraski V, Lass-Flörl C, and Lusser A (2012). CHD1 contributes to intestinal resistance against infection by *P. aeruginosa* in *Drosophila melanogaster*. *PLoS ONE* 7, e43144. [PubMed: 22912810]
- Sebald J, Willi M, Schoberleitner I, Krogsdam A, Orth-Höller D, Trajanoski Z, and Lusser A (2016). Impact of the Chromatin Remodeling Factor CHD1 on Gut Microbiome Composition of *Drosophila melanogaster*. *PLoS ONE* 11, e0153476. [PubMed: 27093431]
- Shechter D, Dormann HL, Allis CD, and Hake SB (2007). Extraction, purification and analysis of histones. *Nat. Protoc* 2, 1445–1457. [PubMed: 17545981]
- Siggens L, Cordeddu L, Rönnerblad M, Lennartsson A, and Ekwall K (2015). Transcription-coupled recruitment of human CHD1 and CHD2 influences chromatin accessibility and histone H3 and H3.3 occupancy at active chromatin regions. *Epigenetics Chromatin* 8, 4. [PubMed: 25621013]
- Simic R, Lindstrom DL, Tran HG, Roinick KL, Costa PJ, Johnson AD, Hartzog GA, and Arndt KM (2003). Chromatin remodeling protein Chd1 interacts with transcription elongation factors and localizes to transcribed genes. *EMBO J.* 22, 1846–1856. [PubMed: 12682017]
- Sims RJ 3rd, Millhouse S, Chen CF, Lewis BA, Erdjument-Bromage H, Tempst P, Manley JL, and Reinberg D (2007). Recognition of trimethylated histone H3 lysine 4 facilitates the recruitment of transcription postinitiation factors and pre-mRNA splicing. *Mol. Cell* 28, 665–676. [PubMed: 18042460]
- Skene PJ, Hernandez AE, Groudine M, and Henikoff S (2009). The nucleosomal barrier to promoter escape by RNA polymerase II is overcome by the chromatin remodeler Chd1. *eLife* 3, e02042.
- Smolle M, Venkatesh S, Gogol MM, Li H, Zhang Y, Florens L, Washburn MP, and Workman JL (2012). Chromatin remodelers Isw1 and Chd1 maintain chromatin structure during transcription by preventing histone exchange. *Nat. Struct. Mol. Biol* 19, 884–892. [PubMed: 22922743]
- Soneson C, Love MI, and Robinson MD (2015). Differential analyses for RNA-seq: transcript-level estimates improve gene-level inferences. *F1000Res.* 4, 1521. [PubMed: 26925227]
- Srinivasan S, Dorigi KM, and Tamkun JW (2008). *Drosophila* Kismet regulates histone H3 lysine 27 methylation and early elongation by RNA polymerase II. *PLoS Genet.* 4, e1000217. [PubMed: 18846226]
- Stockdale C, Flaus A, Ferreira H, and Owen-Hughes T (2006). Analysis of nucleosome repositioning by yeast ISWI and Chd1 chromatin remodeling complexes. *J. Biol. Chem* 281, 16279–16288. [PubMed: 16606615]
- Talbert PB, and Henikoff S (2010). Histone variants-ancient wrap artists of the epigenome. *Nat. Rev. Mol. Cell Biol* 11, 264–275. [PubMed: 20197778]
- Tatar M, Kopelman A, Epstein D, Tu MP, Yin CM, and Garofalo RS (2001). A mutant *Drosophila* insulin receptor homolog that extends life-span and impairs neuroendocrine function. *Science* 292, 107–110. [PubMed: 11292875]

- Torigoe SE, Urwin DL, Ishii H, Smith DE, and Kadonaga JT (2011). Identification of a rapidly formed nonnucleosomal histone-DNA intermediate that is converted into chromatin by ACF. *Mol. Cell* 43, 638–648. [PubMed: 21855802]
- Torigoe SE, Torigoe SE, Patel A, Patel A, Khuong MT, Khuong MT, Bowman GD, Bowman GD, and Kadonaga JT (2013). ATP-dependent chromatin assembly is functionally distinct from chromatin remodeling. *eLife* 2, e00863. [PubMed: 23986862]
- Wang M, Peng I-F, Li S, and Hu X (2020). Dysregulation of antimicrobial peptide expression distinguishes Alzheimer's disease from normal aging. *Aging (Albany NY)* 12, 690–706. [PubMed: 31907335]
- Wickham H (2016). *ggplot2: Elegant Graphics for Data Analysis* (Springer-Verlag).
- Wickham H, François R, Henry L, and Müller K (2020). *dplyr: A Grammar of Data Manipulation*. <https://dplyr.tidyverse.org/reference/dplyr-package.html>.
- Xu Y, Anjaneyulu M, Donelian A, Yu W, Greenberg ML, Ren M, Owusu-Ansah E, and Schlame M (2019). Assembly of the complexes of oxidative phosphorylation triggers the remodeling of cardiolipin. *Proc. Natl. Acad. Sci. USA* 116, 11235–11240. [PubMed: 31110016]
- Zhang Y, Liu T, Meyer CA, Eeckhoutte J, Johnson DS, Bernstein BE, Nusbaum C, Myers RM, Brown M, Li W, and Liu XS (2008). Model-based analysis of ChIP-Seq (MACS). *Genome Biol.* 9, R137. [PubMed: 18798982]
- Zhang H, Gan H, Wang Z, Lee J-H, Zhou H, Ordog T, Wold MS, Ljungman M, and Zhang Z (2017). RPA Interacts with HIRA and Regulates H3.3 Deposition at Gene Regulatory Elements in Mammalian Cells. *Mol. Cell* 65, 272–284. [PubMed: 28107649]
- Zhang K, Rajput SK, Wang S, Folger JK, Knott JG, and Smith GW (2016). CHD1 Regulates Deposition of Histone Variant H3.3 During Bovine Early Embryonic Development. *Biol. Reprod* 94, 1–8.
- Zhu A, Ibrahim JG, and Love MI (2019). Heavy-tailed prior distributions for sequence count data: removing the noise and preserving large differences. *Bioinformatics* 35, 2084–2092. [PubMed: 30395178]

**Highlights**

- Loss of chromatin assembly factor CHD1 reduces H3.3 levels in brain chromatin
- *Chd1* deletion perturbs global chromatin organization similar to *H3.3* deletion
- *Chd1* deletion causes global upregulation of transcription in fly heads
- Brain-specific roles of CHD1 are required for metabolic control and healthy lifespan

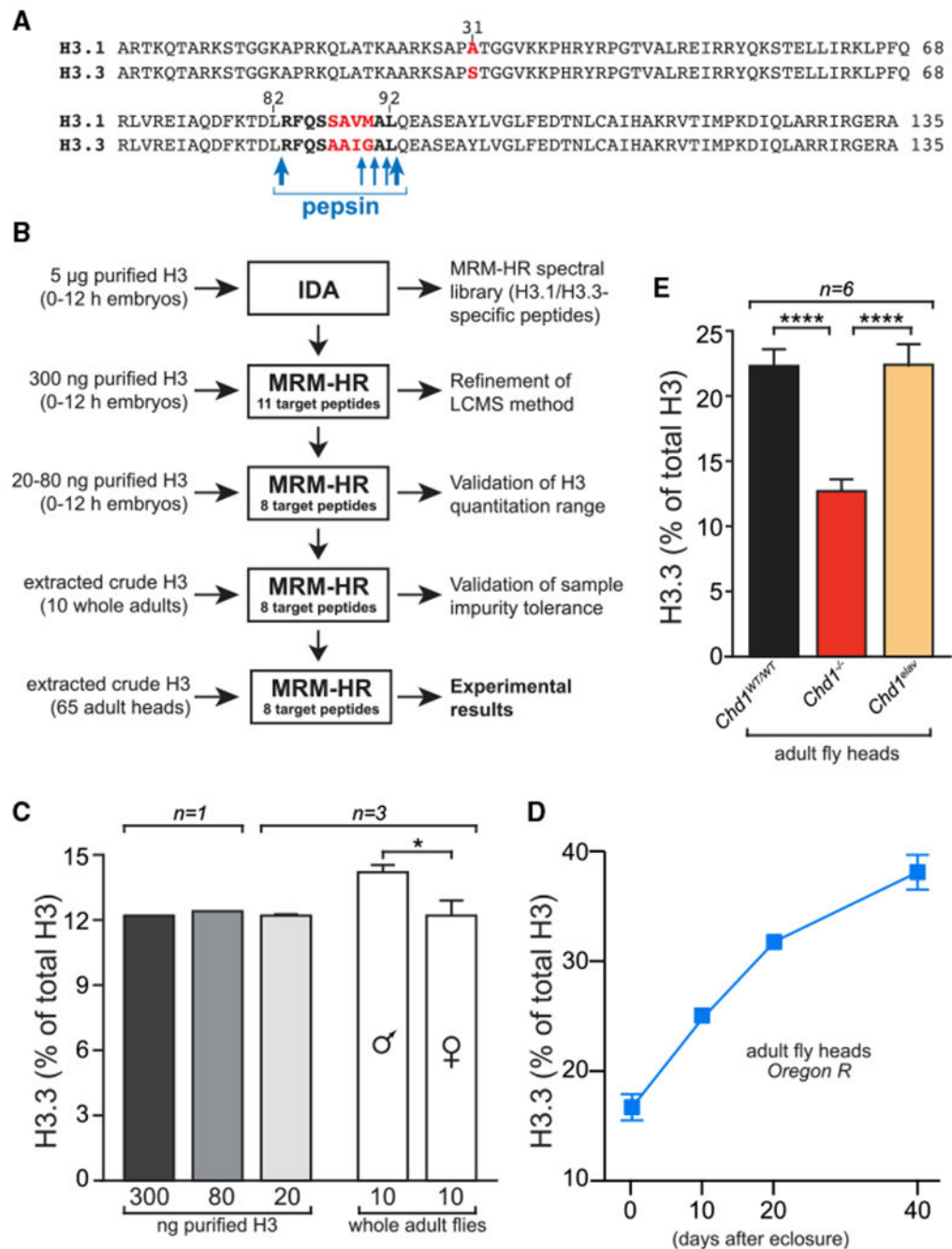


**Figure 1. Quantification of H3.3 in fly heads reveals severely reduced H3.3 levels in the absence of CHD1**

(A) Amino acid sequences of *Drosophila* H3.1 and H3.3. Distinct amino acids are shown in red, major and minor cleavage sites of pepsin around positions 82–92 are marked by bold and thin arrows.

(B) Stepwise refinement of H3.3 quantification by MRM-HR LC-MS/MS.

(C) Quantification of relative amounts of H3.3 in pure embryonic histones and crude preparations of whole adult male and female flies (*Oregon R*). n, number of replicates. Mean  $\pm$  SD is shown.

(D) Quantification of head histones of *Oregon R* flies of the indicated ages (n = 3 pools of 60 heads each).

(E) Relative H3.3 amounts in head chromatin of flies of the indicated genotype. N = 3 (65 heads each of two independent crosses). Mean  $\pm$  SD is shown. Statistical differences in (C) and (E) were calculated by Mann-Whitney test (\*p < 0.05; \*\*\*\*p < 0.0001). See also Figure S1 and Table S1.

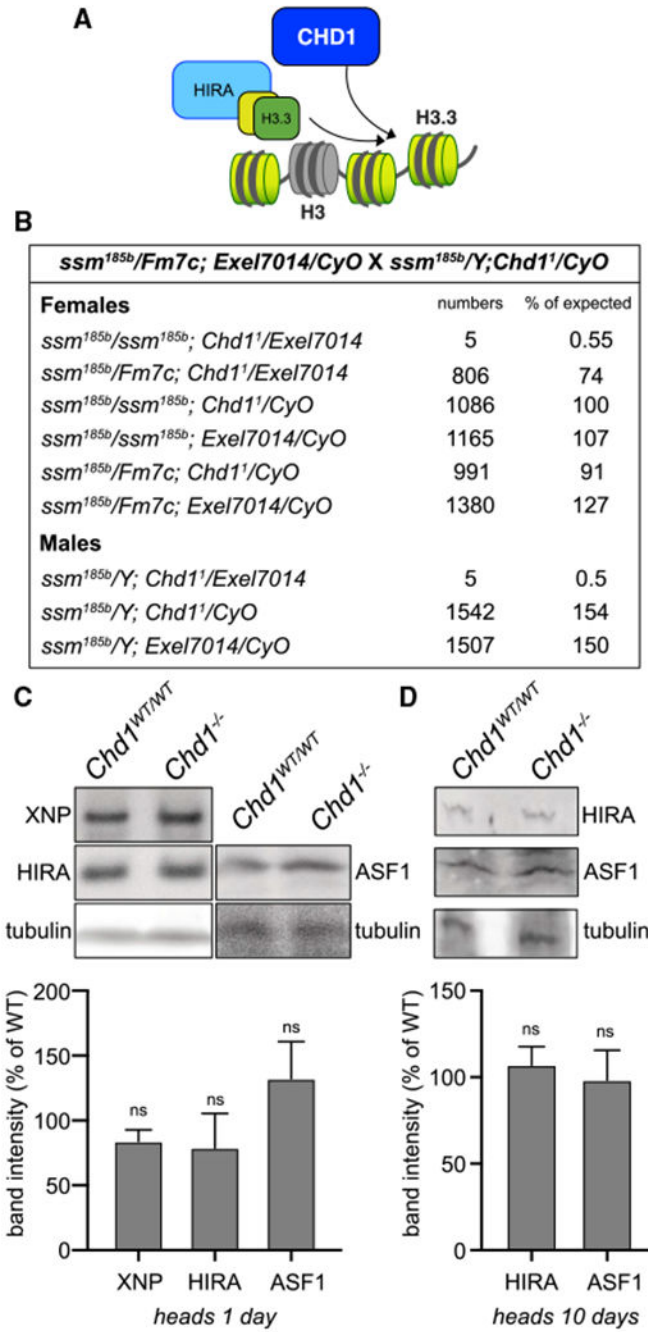


**Figure 2. Cooperation between CHD1 and HIRA in H3.3 incorporation**

(A) Working model for H3.3 incorporation. H3.3 chaperone HIRA delivers and deposits H3.3/H4 histone dimers at sites of histone loss, whereas CHD1 promotes efficient loading and proper spacing of the variant nucleosome.

(B) *Chd1* and *Hira* show synthetic lethal genetic interaction. Absolute numbers of progeny and % of expected Mendelian numbers of the respective genotypes from a cross of heterozygous *Chd1* and *Hira* (*ssm<sup>185b</sup>*) flies are shown.

(C) Protein levels of HIRA, ASF1, and XNP are similar in *Chd1<sup>-/-</sup>* and *Chd1<sup>WT/WT</sup>* heads. Western blot of whole cell extracts from ~100 heads of 1-day-old flies of the indicated genotypes. Tubulin was detected as a loading control (*top*). *Bottom*: quantification of band intensities. Values were normalized to tubulin signals, and mean  $\pm$  SD is shown (N = 3).

Statistical analysis was done by multiple unpaired t test. ns, not significant.

(D) Western blot and quantification as in (C) except that 10-day-old flies were used.

See also Figure S2.

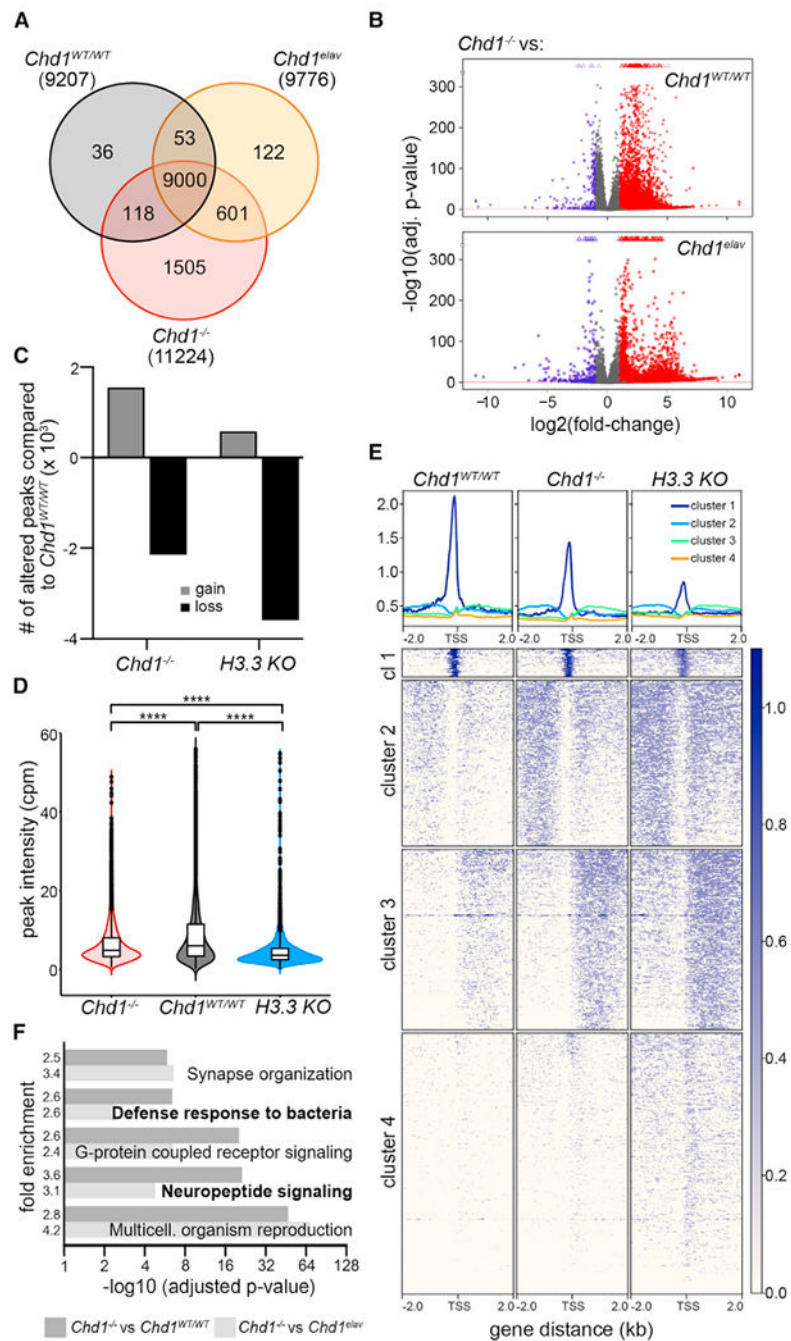


**Figure 3. Deletion of *Chd1* results in global upregulation of brain transcription and chromatin perturbation**

(A) Venn diagram of genes expressed with TPM  $\geq 1$  in heads of flies with the indicated genotype.

(B) Volcano plots of differentially regulated genes in *Chd1*<sup>-/-</sup> heads compared to *Chd1*<sup>WT/WT</sup> and *Chd1*<sup>elav</sup> heads. Color indicates significant (1.2fc  $\geq 1$ , adj. p value  $\leq 0.05$ ) up- (red) or downregulation (blue). Triangles, genes with adj. p value = 0.

(C) ATAC-seq analysis of fly brains shows loss or gain of ATAC-peaks in *Chd1*<sup>-/-</sup> and *H3.3 KO* compared to *Chd1*<sup>WT/WT</sup> flies.

(D) Significantly decreased peak intensities in *Chd1*<sup>-/-</sup> versus *Chd1*<sup>WT/WT</sup> brains (Kruskal-Wallis test; \*\*\*\*p < 0.0001).

(E) Heatmap of normalized ATAC-seq read densities around transcriptional start sites (TSS) reveals clearly enhanced read numbers in gene bodies of *Chd1*<sup>-/-</sup> and *H3.3 KO* brains.

Clusters were identified by k-means clustering.

(F) GO enrichment analysis (biological process) of genes upregulated in *Chd1*<sup>-/-</sup> (12fc 1).

See also Figures S3, S4, and S5 and Tables S2, S3, and S4.

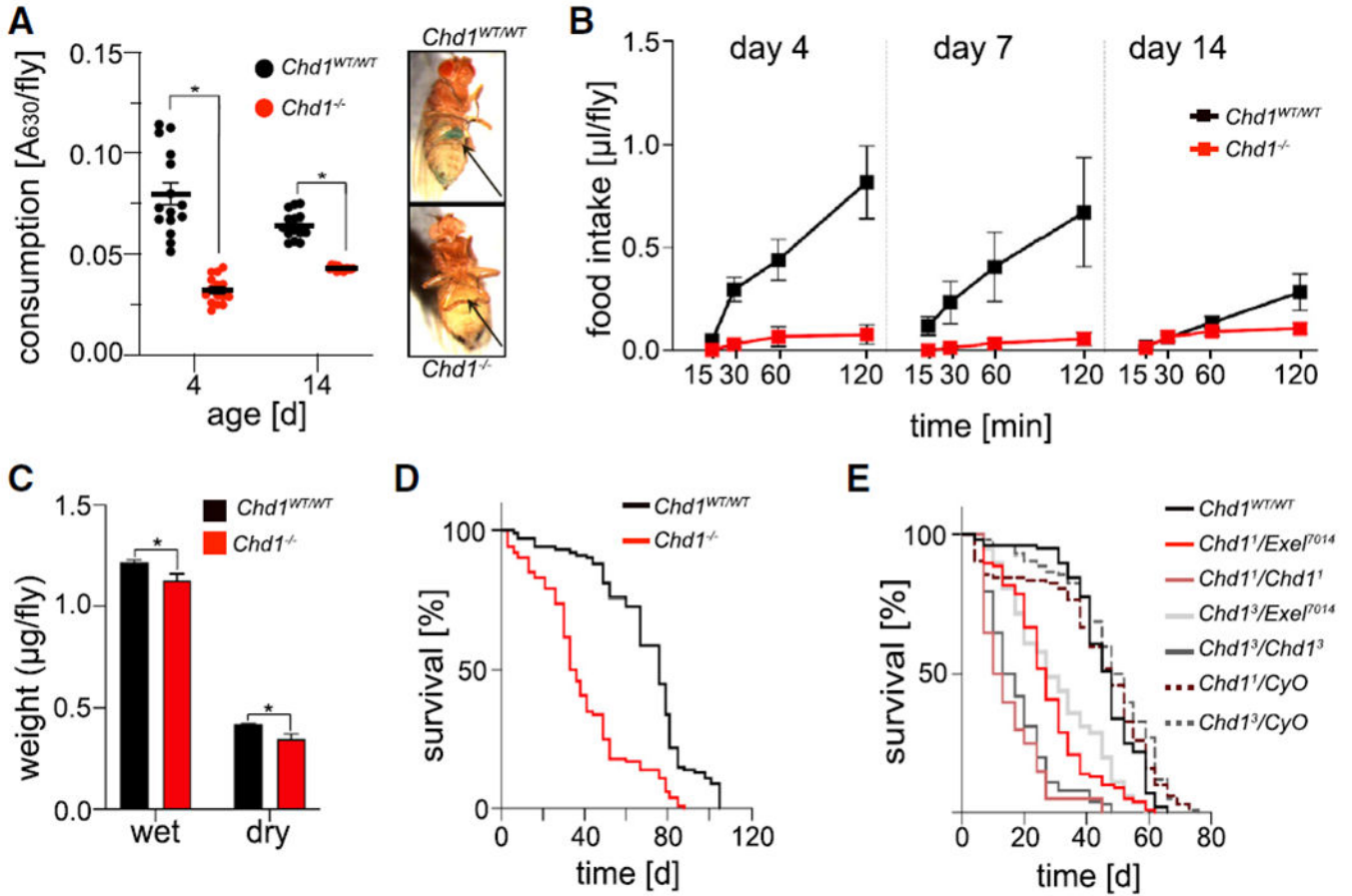


**Figure 4. Deletion of *Chd1* causes lifetime shortening and reduced food intake**

(A) Ingested blue colored food (right panels) was measured photometrically in fly homogenates of 4- and 14-day-old flies and plotted as A<sub>630</sub> absorbance perfly. Statistical significance was calculated by t test (\*p < 0.05). Mean ± SEM is shown (N = 3 with 5 batches of 10 flies each).

(B) Food intake of 4-, 7-, and 14-day-old virgin females was measured by CAFE assay and food intake per fly was calculated. Mean ± SD is shown for 6 batches of 20 flies each. 3-way ANOVA revealed significant differences between genotypes (F[1,14] = 24.18, p = 0.0002), ages (F[1,14] = 8.923, p = 0.0098), and time point of measurement (F[1.200,16.80] = 45.35, p < 0.0001). Genotype × age × measurement time point effect: F[3,42] = 8.092, p = 0.0002.

(C) Wet and dry weight of *Chd1*<sup>WT/WT</sup> and *Chd1*<sup>-/-</sup> flies (unpaired t test; n = 50; \*p < 0.05). Mean ± SD is shown.

(D) Survival curves of *Chd1*<sup>WT/WT</sup> and *Chd1*<sup>-/-</sup> flies (n > 200 per genotype).

(E) Survival curves of *Chd1*<sup>WT/WT</sup> flies and flies with different combinations of mutant *Chd1* alleles (n > 60 per genotype).

See also Figure S6.

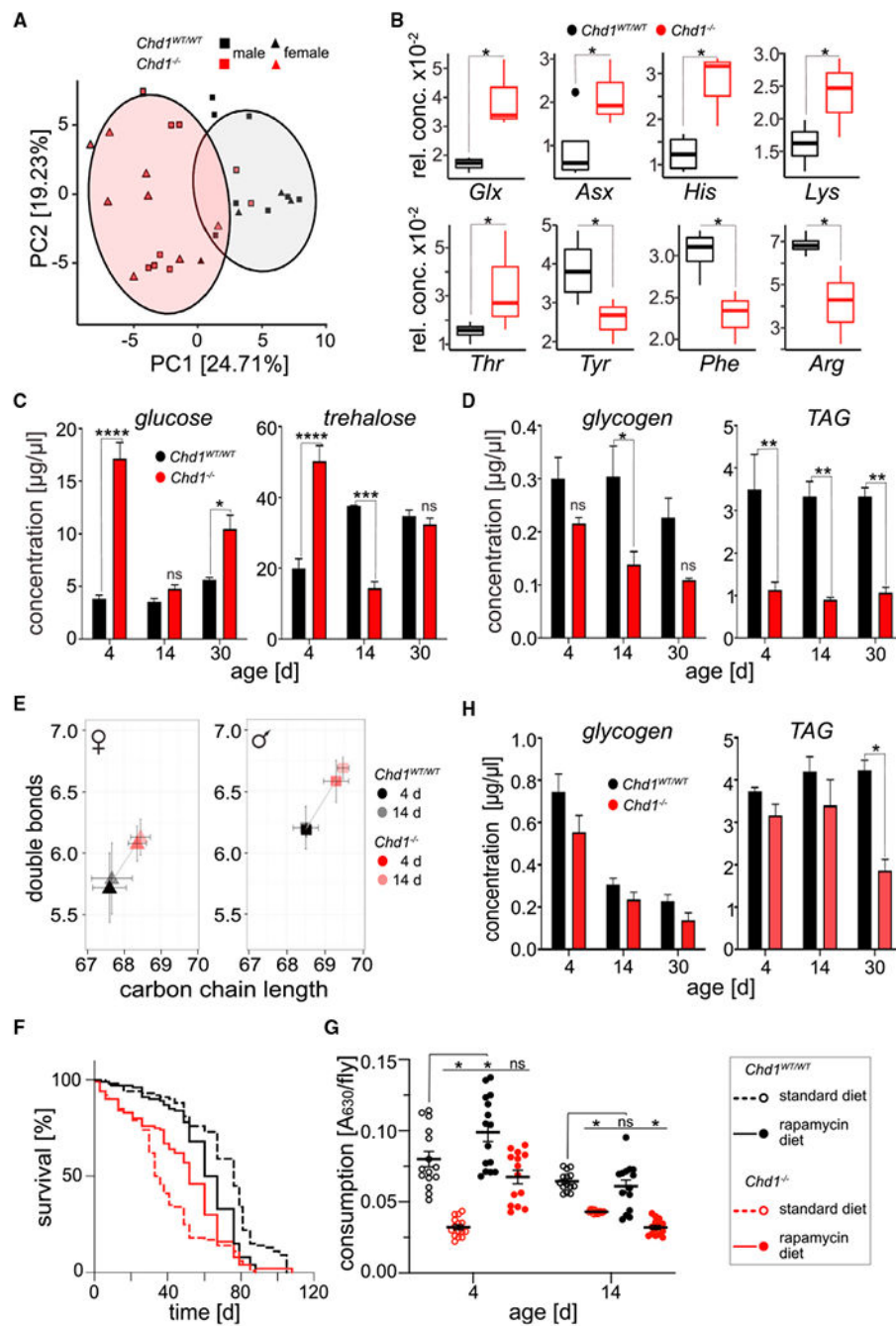


**Figure 5. *Chd1* deletion disturbs global metabolism**

(A) Global metabolic profiling shows segregation of *Chd1*<sup>WT/WT</sup> and *Chd1*<sup>-/-</sup> samples (red and gray ellipses; unpaired t test with Welch's correction;  $p = 6.992 \times 10^{-4}$ ). 87 features of 29 samples of 4- and 14-day-old female and male flies (see also Figure S7) were subjected to PCA analysis.

(B) Global abundance of the indicated amino acids in *Chd1*<sup>WT/WT</sup> and *Chd1*<sup>-/-</sup> flies. Males and females as well as age groups were combined for this analysis. Median concentrations  $\pm$  SD and outliers (dots) normalized to total amino acid concentration are shown ( $n = 4$

*Chd1*<sup>-/-</sup> and  $n = 3$  *Chd1*<sup>WT/WT</sup>). Statistical analysis was performed by Tukey-HSD t test (\* $p < 0.05$ ).

(C) Levels of circulating glucose and trehalose were determined in hemolymph from flies of the indicated age.

(D) Glycogen and TAG were tested in fly extracts. Mean  $\pm$  SEM is shown in (C) and (D) ( $N = 3$  with 3 batches of 50 flies each). Statistical analysis was done by 2-way ANOVA and Tukey post hoc test (\* $p < 0.05$ , \*\* $p < 0.01$ , \*\*\* $p < 0.001$ , \*\*\*\* $p < 0.0001$ , ns, not significant).

(E) Quantification of mitochondrial cardiolipin composition by LC-MS/MS in female (left) and male (right) *Chd1*<sup>-/-</sup> and *Chd1*<sup>WT/WT</sup> flies ( $n = 5$  batches of 20 flies per age, sex, and genotype). Mean  $\pm$  SD is shown.

(F) Survival curves of *Chd1*<sup>WT/WT</sup> and *Chd1*<sup>-/-</sup> flies reared on standard diet or diet supplemented with 200  $\mu$ M rapamycin.

(G) Food intake on standard or rapamycin-supplemented diet. Quantification and statistical analysis as in Figure 4A ( $N = 3$  with 5 batches of 10 flies each) \* $p < 0.05$ ; ns, not significant.

(H) Glycogen and TAG in homogenates of flies kept on rapamycin-supplemented diet were measured as in (D).

See also Figures S7, S8 and S9 and Tables S5 and S6.

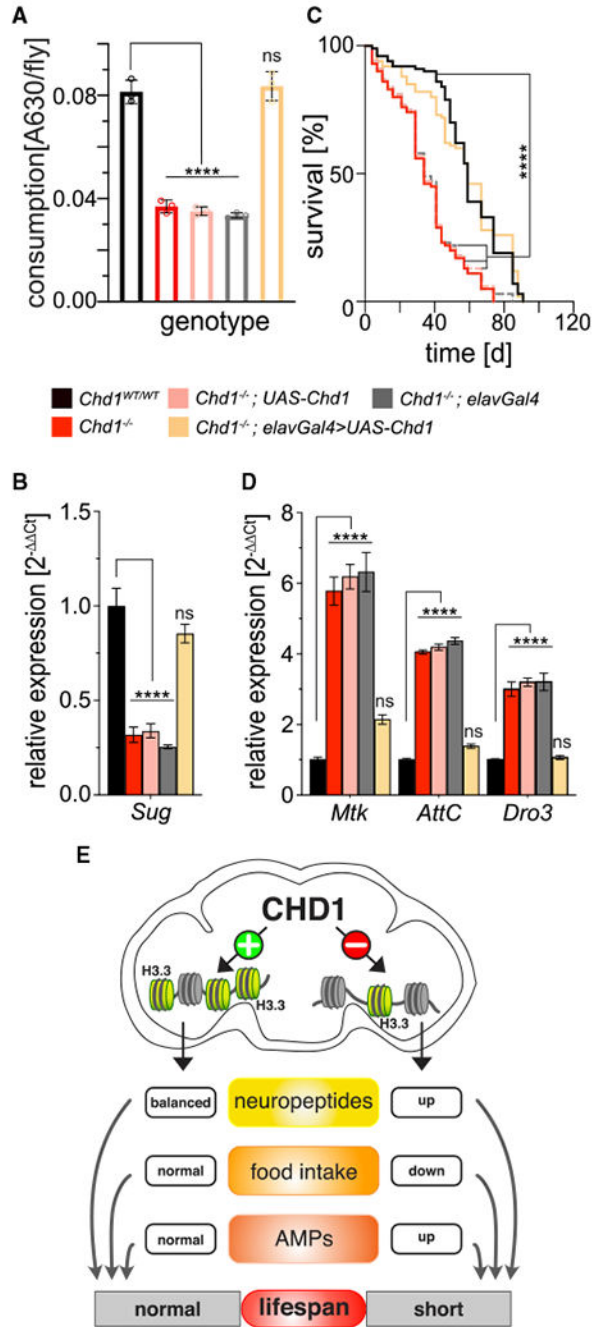


**Figure 6. Pan-neural expression of *Chd1* fully rescues lifespan and consumption defects**  
 (A) Food intake by 7-day-old flies was measured as described in Figure 4A. Statistical analysis was performed by one-way ANOVA (\*\*\*\* $p < 0.0001$ ; ns, not significant).  
 (B) RT-qPCR analysis of the glycogen and lipid storage regulator gene *Sug* with abdominal RNA from 7-day-old flies. Transcript levels were normalized to *Actin* and expressed relative to *Chd1<sup>WT/WT</sup>* flies. Mean  $\pm$  SEM are shown (N = 3 with 100 flies each; unpaired t test: \*\*\*\* $p < 0.0001$ ; ns, not significant).

(C) Survival curves of *Chd1<sup>WT/WT</sup>*, *Chd1<sup>-/-</sup>*, *Chd1<sup>elav</sup>*, and the respective *UAS* and *Gal4* control flies. Comparison of survival curves was done by Mantel-Cox test (n > 60 per genotype). Statistically significant differences were observed between *Chd1<sup>WT/WT</sup>* and all other strains except *Chd1<sup>elav</sup>* (\*\*\*\*p < 0.0001).

(D) RT-qPCR analysis of antimicrobial peptide genes was performed as described in (B).

(E) Model for the action of CHD1 in maintaining chromatin structure in the brain, in particular by incorporating H3.3, to ensure proper regulation of neuropeptide expression. In the absence of CHD1, H3.3 incorporation is reduced, leading to general transcriptional upregulation of neuropeptides and other genes, which in turn compromises feeding behavior, disrupts metabolic homeostasis, and leads to increased inflammation (AMP expression) ultimately resulting in lifespan shortening.

**Table 1.***Drosophila* strains used in this study

Strain name	Genotype	Source
<i>Chd1<sup>WT/WT</sup></i>	<i>w<sup>1118</sup>, Chd1<sup>1</sup>, P{Chd1<sup>+</sup>}/Df(2L)Exel<sup>7014</sup>, P{Chd1<sup>+</sup>}</i>	Morettini et al., 2011
<i>Chd1<sup>-/-</sup></i>	<i>w<sup>1118</sup>, Chd1<sup>1</sup>/Df(2L)Exel<sup>7014</sup></i>	Konev et al., 2007
<i>UAS-Chd1</i>	<i>w<sup>111</sup>; Chd1<sup>1</sup>, P{w<sup>+</sup>, UAS-Chd1}/Df(2L)Exel<sup>7014</sup></i>	Konev et al., 2007
<i>elav-Gal4</i>	<i>w<sup>1118</sup>, Chd1<sup>1</sup>/Df(2L)Exel<sup>7014</sup>, P{w<sup>+</sup>, elav-Gal4}/+</i>	this study
<i>Chd1<sup>elav</sup></i>	<i>w<sup>1118</sup>, Chd1<sup>1</sup>, P{w<sup>+</sup>, UAS-Chd1}/Df(2L)Exel<sup>7014</sup>, P{w<sup>+</sup>, elav-Gal4}/+</i>	this study
<i>H3.3KO</i>	<i>w<sup>1118</sup>, delH3.3B(w<sup>+</sup>) hsp-Flp/delH3.3B(w<sup>+</sup>) hsp-Flp, Df(2L)H3.3A/Df(2L)H3.3A</i>	Hödl and Basler, 2009
<i>ssm<sup>185b</sup></i>	<i>w<sup>1118</sup>, ssm<sup>185b</sup>/FM7c</i>	Loppin et al., 2000
<i>UAS-2xsNPF</i>	<i>w<sup>1118</sup>, UAS-sNPF; UAS-sNPF</i>	Lee et al., 2008
<i>Chd1<sup>sNPF</sup></i>	<i>w<sup>1118</sup>, Chd1<sup>1</sup>, UAS-sNPF/Df(2L)Exel<sup>7014</sup>, P{w<sup>+</sup>, elav-Gal4}/UAS-sNPF</i>	this study

## KEY RESOURCES TABLE

REAGENT or RESOURCE	SOURCE	IDENTIFIER
<b>Antibodies</b>		
rabbit $\alpha$ -dmXNP15879 antibody	Emelyanov et al., 2010	N/A
rabbit $\alpha$ -dmHIRA antibody	Konev et al., 2007	N/A
rabbit $\alpha$ -dmASF1 antibody	Jessica Tyler, Weill Cornell Medicine	N/A
mouse $\alpha$ -tubulin antibody	Sigma Aldrich	RRID: AB_477579
HRP-coupled secondary antibody mouse	Sigma Aldrich	RRID: AB_259755
HRP-coupled secondary antibody rabbit	Sigma Aldrich	RRID: AB_258103
<b>Chemicals, peptides, and recombinant proteins</b>		
NaCl	Roth	Cat#39572
HEPES-KOH	Roth	Cat#9105.3
EDTA	Sigma Aldrich	Cat#E6760
NP-40	Sigma Aldrich	Cat#I3021
UltraPure Sucrose	Invitrogen	Cat#15503022
Propidium iodide	Sigma Aldrich	Cat#P4170
MgCl <sub>2</sub>	Roth	Cat#2189,1
H <sub>2</sub> SO <sub>4</sub>	Merck	Cat#30743
Acetone	Roth	Cat#9372.2
Tris base	Sigma Aldrich	Cat#GE17-1321-01
Trichloroacetic acid (TCA)	Merck	Cat#8071000
Ammonium bicarbonate (ABC)	Merck	Cat#101131
Acetonitrile (ACN)	Bartlet	Cat#CL0001752500
Dithiothreitol (DTT)	Roth	Cat#6908.3
Iodoacetamide (IAA)	Sigma Aldrich	Cat#I-6125
Pepsin	Promega	Cat#V1959
SDS	Roth	Cat#2326.5
Glycerol	Roth	Cat#3783.1
2-mercapto-ethanol	Roth	Cat#4227.3
TRI Reagent	Sigma Aldrich	Cat#T-9424
DNase I	New England Biolabs	Cat#M0303
Igepal CA-630	Sigma Aldrich	Cat#I8896
cOmplete, EDTA-free protease inhibitor cocktail	Roche	Cat#COEDTAF-RO
Q5 High-Fidelity DNA Polymerase	New England Biolabs	Cat#E0555
Tegosept	Sigma Aldrich	Cat#54680
Rapamycin from <i>Streptomyces hygroscopicus</i>	Sigma Aldrich	Cat#R0395
Triton X-100	Acros Organics	Cat#215682500
E133 brilliant blue food coloring	Sigma Aldrich	Cat#80717
Porcine trehalase	Sigma Aldrich	Cat#T8778

REAGENT or RESOURCE	SOURCE	IDENTIFIER
Amyloglycosidase	Sigma Aldrich	Cat#A7095
<b>Critical commercial assays</b>		
Luna® Universal qPCR Master Mix	New England Biolabs	Cat#M3003
LunaScript RT SuperMix Kit	New England Biolabs	Cat#E3010
GE Healthcare Amersham ECL Prime Western-Blot Detection	GE Healthcare	Cat#28980926
Illumina Tagment DNA Enzyme and Buffer	Illumina	Cat#20034197
Monarch Genomic DNA Purification Kit	New England Biolabs	Cat#T3010
Monarch PCR & DNA Cleanup Kit	New England Biolabs	Cat#T1030
Glucose (HK) assay kit	Sigma Aldrich	Cat#GAHK20
Serum Triglyceride Detection Kit	Sigma Aldrich	Cat#TR0100
<b>Deposited data</b>		
ATAC-seq raw data	Sequence Read Archive SRA	<a href="#">SRA: PRJNA730408</a>
RNA-seq data	Gene Expression Omnibus repository	<a href="#">GEO: GSE146392</a>
<b>Experimental models: organisms/strains</b>		
<i>Drosophila melanogaster</i> : <i>Chd1</i> <sup>WT/WT</sup> ; <i>w</i> <sup>1118</sup> ; <i>Chd1</i> <sup>1</sup> , <i>P{Chd1<sup>+</sup>}/Df(2L)Exel<sup>7014</sup></i> , <i>P{Chd1<sup>+</sup>}</i>	Moretini et al., 2011	N/A
<i>Drosophila melanogaster</i> : <i>Chd1</i> <sup>-/-</sup> ; <i>w</i> <sup>1118</sup> ; <i>Chd1</i> <sup>1</sup> / <i>Df(2L)Exel<sup>7014</sup></i>	Konev et al., 2007	N/A
<i>Drosophila melanogaster</i> : <i>UAS-Chd1</i> ; <i>w</i> <sup>1118</sup> ; <i>Chd1</i> <sup>1</sup> , <i>P{w<sup>+</sup>, UAS-Chd1}/Df(2L)Exel<sup>7014</sup></i>	Konev et al., 2007	N/A
<i>Drosophila melanogaster</i> : <i>elav-Gal4</i> ; <i>w</i> <sup>1118</sup> ; <i>Chd1</i> <sup>1</sup> / <i>Df(2L)Exel<sup>7014</sup></i> ; <i>P{w<sup>+</sup>, elav-Gal4}/+</i>	<i>this study</i>	N/A
<i>Drosophila melanogaster</i> : <i>Chd1</i> <sup>elav</sup> ; <i>w</i> <sup>1118</sup> ; <i>Chd1</i> <sup>1</sup> , <i>P{w<sup>+</sup>, UAS-Chd1}/Df(2L)Exel<sup>7014</sup></i> ; <i>P{w<sup>+</sup>, elav-Gal4}/+</i>	<i>this study</i>	N/A
<i>Drosophila melanogaster</i> : <i>H3.3KO</i> ; <i>w</i> <sup>1118</sup> , <i>delH3.3B(w<sup>+</sup>)</i> , <i>hsp-Flp</i> ; <i>Df(2L)H3.3A/SM6B</i>	Hödl and Basler, 2009	N/A
<i>Drosophila melanogaster</i> : <i>Ssm</i> <sup>185b</sup> ; <i>w</i> <sup>1118</sup> , <i>ssm 185b/FM7c</i>	Loppin et al., 2000	N/A
<i>Drosophila melanogaster</i> : <i>UAS-2xsNPF</i> ; <i>w</i> <sup>1118</sup> ; <i>UAS-sNPF</i> ; <i>UAS-sNPF</i>	Lee et al., 2004	N/A
<i>Drosophila melanogaster</i> : <i>Chd1</i> <sup>sNPF</sup> ; <i>w</i> <sup>1118</sup> ; <i>Chd1</i> , <i>UAS-sNPF/Df(2L)Exel<sup>7014</sup></i> ; <i>P{w<sup>+</sup>, elav-Gal4}/UAS-sNPF</i>	<i>this study</i>	N/A
<i>Drosophila melanogaster</i> : <i>Oregon R</i> ; <i>w</i> <sup>+O</sup>	<i>this study</i>	N/A
<b>Oligonucleotides</b>		
Ad1_noMX	Buenrostro et al., 2013	N/A
Ad2.1-Ad2.3	Buenrostro et al., 2013	N/A
Ad2.7-Ad2.12	Buenrostro et al., 2013	N/A
<b>Software and Algorithms</b>		
Skyline Spectral Library	MacCoss Lab Software	v20.1.0.155
Fusion Software	PeqLab	v15.17
R	<a href="https://www.r-project.org">https://www.r-project.org</a>	v3.6.1
deepTools suite	Ramírez et al., 2014	v3.5.1
GraphPad Prism	GraphPad	v8.2.1